Understory Light Availability and Spatial Variation

Miranda Fix

A thesis

submitted in partial fulfillment of the

requirements for the degree of

Master of Science

University of Washington

2013

Committee:

E. David Ford

Vladimir Minin

Program Authorized to Offer Degree:

Quantitative Ecology and Resource Management

University of Washington

Abstract

Understory Light Availability and Spatial Variation

Miranda Fix

Chair of the Supervisory Committee:

Professor E. David Ford

Quantitative Ecology and Resource Management

Photosynthetically active radiation is a critical resource for understory plants and its availability and heterogeneity plays a major role in seedling regeneration and survival. This thesis examines various methods to quantify understory light availability, temporal dynamics and spatial variation in a shaded environment. Comparing indirect estimates to direct measurements by BF3 sensors, we found that hemispherical image analysis (HIA) overestimated the proportion of total and diffuse light transmitted to the understory. Instantaneous BF3 readings were correlated to daily integrative BF3 estimates, but were subject to outliers depending on sky condition. The median of several ten-minute means performed better than other indirect estimates. We used the BF3 sensor to develop a new definition of sunflecks and to quantify the distribution of sunfleck duration and peak intensity in our study plot. In addition, we characterized spatial variation in understory light using both HIA and a mobile BF3 sensor system. Our results highlight temporal variation in spatial patterns, even for diffuse transmittance over a short period of time.

TABLE OF CONTENTS

Page

LIST OF FIGURES

LIST OF TABLES

ACKNOWLEDGEMENTS

This work would not be possible without the help and support of many people. I am grateful to my advisor, David Ford, for the opportunity to work on this project and in particular to gain fieldwork experience, and Vladimir Minin for serving on my committee and providing valuable feedback. I would like to thank past and present members of the Canopy Dynamics Lab for their continual support: Shawn Behling, Amita Banerjee, Ziyu Ma and Bert Loosmore, as well as our lab assistant extraordinaire, Danaan Deneve Weeks, who turned the vision of a mobile sensor system into a reality.

Theresa Santman, Deric Kettel, and Jason Cross from the Olympic Natural Resources Center provided logistical and technical support during the field season, as did Marc Morrison, Stephen Williams at Delta-T Devices, and Erik Gjesfjeld from the UW Archaeology Department. I was lucky to work with such wonderful field assistants as Jennifer Apple, Andrew Annanie and Thien-Y Le. It was a pleasure to discuss statistical issues with Paul Sampson and I appreciate his advice. A number of researchers were kind enough to respond to my inquiries about their work, including Dennis Baldocchi, Eben Broadbent, Eric Graham, Doug Sprugel, and Lee Vierling.

I am grateful for all the funding that has supported me these past few years, including research funding from the US Forest Service and teaching assistantships through CQS and the Statistics Department, as well as travel funding from the ASA. Thank you to QERM not only for funding but also for an amazing community that brought me here in the first place. Joanne Besch and Amanda Davis deserve special thanks for their help in practical matters. Finally, I would like to thank my friends and family for all their love and support, especially my parents Charlotte and Douglas, my roommates Jenn and Kiva, my buddies Colin and Joming, and my partner David.

Chapter 1

INTRODUCTION

Light interception is critical to forest stand development and the establishment of saplings in the understory, and is often considered in predicting establishment and growth of regeneration following partial cutting. While managers have no control over above-canopy light, they can control understory light by controlling the amount, position and type of vegetation. Benefits from controlling understory light may include promoting establishment and early development of tree seedlings as well as controlling shrub or herb layers either to suppress their growth as competitors or to promote their growth for wildlife habitat or biodiversity reasons (Lieffers et al., 1999). For example, one of the management objectives in our study region is to create a multi-tiered canopy in stands that currently only have a single tier. A key question is how to control light levels such that adequate regeneration occurs and a lower tier of canopy develops without forming a dense thicket requiring extensive management.

Given knowledge of the requirements of desired species and their physiological responses to different light levels, it should be possible to identify the range, spatial and temporal distribution of understory light most appropriate for growth and survival of these species. This information would enable managers to achieve their goals more consistently and efficiently (Grayson et al., 2012). However, in order to provide such target light conditions, we must first be able to accurately characterize existing understory light environments. Understory light varies in space and time and is influenced by myriad factors such as the solar path, sky conditions, stand density and structure, leaf phenology, canopy height, and foliage movement due to wind (Messier et al., 1998; Gendron et al., 1998). Each point underneath the canopy receives both

direct light from the sun and diffuse light which has been scattered by molecules and particles in the atmosphere. The relative proportions of direct and diffuse light vary depending on cloudiness – most of the light available on overcast days is diffuse. In addition, light can be reflected or transmitted by vegetation. All this complexity and variability poses challenges to characterizing understory light environments.

The present study examines various methods to quantify understory light availability, temporal dynamics and spatial variation in a low-light environment. In Chapter 2, we compare direct measurements of understory light availability using the BF3 sunshine sensor to indirect estimates from instantaneous readings as well as hemispherical image analysis. We also use the ability of the BF3 sensor to directly measure diffuse light to establish a new definition of sunflecks, and apply this definition to describe sunfleck characteristics. In Chapter 3, we investigate spatial variation in understory light availability using both hemispherical image analysis and a mobile BF3 sensor system and discuss the utility of constructing spatial maps of understory light.

Chapter 2

EVALUATING VARIOUS METHODS TO ESTIMATE UNDERSTORY LIGHT AVAILABILITY UNDER A DENSE CANOPY

2.1 Introduction

Solar radiation between 400 and 700 nm (photosynthetically active radiation or PAR) is one of the most important resources for plants, due to its central role in photosynthesis and other plant processes. Photosynthetic photon flux density (PPFD, $\mu mol/m^2/s$) in the corresponding waveband is the most commonly used unit to characterize PAR, and is hereafter simply referred to as 'light.' Light availability beneath a heterogeneous forest canopy is difficult to quantify because of its large spatial and temporal variability (Baldocchi and Collineau, 1994). Various methods have been used to characterize this complex understory light environment. Most of these methods estimate the proportion of incident PPFD transmitted through the canopy in order to compare light availability under different conditions (Gendron et al., 1998). In the present study we will refer to this transmitted proportion as 'transmittance.'

A standard method of directly measuring transmittance involves leaving a light sensor coupled to a data-logger in a given understory location, while another sensor is positioned above the canopy to measure incident light. Typically the sensors used are LI-COR Li-190SA quantum sensors or gallium-arsenide-phosphide (GaAsP) photodiodes. Researchers agree that direct readings by light sensors give the most accurate measure of light at a specific place and time. Ideally measurements should be made continuously over an extended period of time, such as the growing season, in order to sample the spatial and temporal complexity of the light environment (Englund et al., 2000; Gendron et al. 1998). However, this is not practical for most research because it is costly and time-consuming. The number of microsites that can be sampled is limited

by the number of sensors (Comeau et al., 1998; Engelbrecht and Herz, 2001). To overcome these drawbacks of direct measurement, much effort has been directed toward development and evaluation of various methods for the indirect estimation of light availability (see Table 2.1).

One such indirect method is hemispherical image analysis (HIA), where a photograph is taken looking up into the canopy through a fisheye lens. This photograph records the geometry of the canopy above a given point in the understory, and can be analyzed with computer software to estimate transmittance for any specified period of time. Due to a plethora of factors affecting image grey tones (e.g. exposure, gamma correction, and heterogeneity of sky irradiance) Evans and Coombe (1959) concluded that "*any attempt to use [HIA] as a means of measuring the transmission of the canopy directly would be so uncertain as not to be worth the labour involved.*" Since then protocols have been developed to improve comparability of results, but HIA still requires significant user input and the time and skills to analyze the photographs (Paquette et al., 2007). To avoid large variation in brightness across the image, photographs are taken beneath a uniformly overcast sky, or at dawn or dusk (Hale and Edwards, 2002), which is quite restrictive. In recent years, digital photographs have been widely used as a faster and less expensive substitute for film photographs. Several studies have shown that the digital format can provide comparable results to film (Hale and Edwards, 2002; Rozenbergar et al., 2011).

While several studies have found a high level of agreement between transmittance estimates from HIA and direct measurements made by light sensors (e.g. Comeau et al. 1998; Engelbrecht and Herz, 2001; Gendron et al., 1998, Promis et al., 2012, Rich et al., 1993), others have found that predictions are not always independent of forest type or condition, and lack of repeatability can make it difficult to compare sites and studies (Clearwater et al., 1999). Some

comparisons against direct measurements have found HIA unable to discriminate between differences in transmittance beneath dense canopies, where the transmittance falls below 10% (e.g. Hale and Edwards, 2002; Machado and Reich, 1999; Roxburgh and Kelly, 1995). A possible reason might be that measurement error exceeds actual differences in transmittance. This is problematic because transmittance is often in the 1-3% range beneath closed-canopy forest and 5-10% in small gaps (Canham et al., 1990). Accurate assessment of light availability in moderate to deep shade is important for understanding adaptations to shade, which is a key factor underlying the dynamics of forest succession (Machado and Reich, 1999). Characterizing the spatial variation of understory light also requires being able to distinguish between microsites, or at least accurately rank them. Rozenbergar et al. (2011) suggested that more work should be done to assess the performance of HIA at the low end of the radiation spectrum.

Another common method to indirectly estimate transmittance is the instantaneous measurement with light sensors above and below the canopy. Single measurements taken at midday in midsummer have been used to characterize overall light environments (Comeau et al., 1998). Messier and Puttonen (1995) found that single measurements on sunny days gave highly variable results because of the interplay of sun position and gap location. Parent and Messier (1996) therefore recommended that instantaneous measurements be taken on overcast days (the 'Overcast method'). They found overcast measures to be strongly and directly related with mean daily transmittance values. Some studies have also used 10-minute averages on overcast days instead of a single reading (e.g. Gendron et al., 1998; Tobin and Reich, 2009).

Paquette et al. (2007) proposed a less restrictive alternative to the Overcast method, namely using the BF2 type Sunshine Sensor (Delta-T Devices, Cambridge, UK) to make the

instantaneous measurements instead of previously used quantum sensors or GaAsP photodiodes. The BF2 and subsequent models (BF3, BF5) directly measure both diffuse and total light components with an array of seven cosine-corrected photodiodes arranged under a patterned, hemispherical dome. The pattern of clear and opaque areas on the dome is matched to the pattern of photodiodes in such a way that at least one photodiode is always exposed to the full solar beam, at least one photodiode is always completely shaded, and all photodiodes receive an equal sampling of diffuse light from the sky hemisphere (Wood et al., 2003). Using only the diffuse light component, Paquette et al. (2007) found that instantaneous estimates of transmittance made by the BF2 under variable sky conditions were strongly correlated to the those from the Overcast method. However, they did not actually use the BF2 to characterize light conditions over any extended period of time.

In the present study, we use continuous direct measurements from BF3 sensors to calculate daily integrative estimates of transmittance under a dense *Tsuga heterophylla* canopy. Working in a similar environment, Ma (2010) suggested that HIA overestimated transmittance relative to BF3 readings. The first objective of our study was to investigate this more thoroughly by comparing daily integrative BF3 estimates to several versions of indirect estimates made by HIA. Our second objective was to evaluate the method of Paquette et al. (2007) by comparing daily integrative BF3 estimates to instantaneous BF3 estimates of transmittance. Overall, we were especially interested in diffuse transmittance since it may be a better predictor of growth (Kobe and Hogarth, 2007; Tang et al., 1992). A third objective of this study was to use our continuous BF3 measurements to characterize the complex light microclimate at our study site, including the characteristics and contributions of direct light events (sunflecks) in the understory.

		Direct measurements			Indirect measurements					
Study	**Habitat Type**	QS (integ)	GaAsP	BF# (integ)	QS (inst)	BF# (inst)	HIA (film)	HIA (digital)	LAI-2000	Spherical densiometer
Rich et al. 1993	Tropical forest		X				X			
Parent and Messier 1996	Spruce-birch (Quebec)	X			X					
Comeau et al. 1998	Paper birch (B.C.)	X					X		X	X
Gendron et al. 1998	Bigleaf maple (B.C.)		X		10-min means		X		X	
Clearwater et al. 1999	Tropical rain forest	X					X			
Machado and Reich 1999	Various		X		X		X		X	
Englund et al. 2000	Tropical forest						X	X		X
Engelbrecht and Herz 2001	Tropical forest	X	X				X and 24 mm	38 mm	X	X
Ferment et al. 2001	Tropical forest						X		X	X
Frazer et al. 2001	Coastal forest (B.C.)						X	X		
Hale and Edwards 2002	Coniferous forest (Scotland)						X	X		
Kobe and Hogarth 2007	Deciduous forest		X				X	X	X	
Minkova and Logan 2007	Grand-fir and Douglas-fir							X		X
Paquette et al. 2007	Deciduous forest				X	X		X		
Tobin and Reich 2009	Old-growth (Michigan)		X		10-min means				X	
Rozenbergar et al. 2011	Silver-fir-beech (Slovenia)						X	X	X	
Promis et al. 2012	Lenga beech (Chile)	X						X		
Present study	Western hemlock			X		X		X		

Table 2.1 Studies comparing methods to quantify understory light, adapted from Kobe and Hogarth (2007).

2.2 Methods

2.2.1 Study area

The study was conducted in a forest stand on the west side of the Olympic Peninsula (47º49'49" N, 124º15'25" W, Fig. 2.1) managed by the Washington State Department of Natural Resources. Soils were formed from the deposits of alpine glaciers (Tabor and Cady, 1978) and the site is generally level with an elevation of 180 m. Mean annual precipitation in the Hoh River watershed ranges from 2500 to over 5000 mm, and mean air temperature ranges from -1.4ºC in January to 26ºC in July (DeFerrari and Naiman, 1994). The stand is located on the boundary of the *Picea sitchensis* and *Tsuga heterophylla* zones (Franklin and Dyrness, 1973) and dominated by an even-aged *T. heterophylla* cohort naturally regenerated after a major wind disturbance in 1921. During April to September, this region receives the fewest sunshine hours in the continental United States (Geological Survey, 1968) and some 25% less than most of the *Tsuga* zone. Regenerating conifer saplings in the forest understory are largely *Abies amabilis* and *Tsuga heterophylla* with occasional *Thuja plicata* and *Picea sitchensis*.

Fig. 2.1 Study location on the west side of the Olympic Peninsula, Washington State (source: Google Earth).

All measurements were taken within a 50 x 50 m square plot representative of the portion of the stand that has not been thinned since the establishment of the dominant cohort in 1921. The study plot was laid out using a total station surveying instrument, and plot size was chosen based on results from a pilot study in Summer 2011. All trees greater than 10cm diameter at breast height (dbh) were mapped on an x-y grid system to the nearest centimeter (Fig. 2.2a) and measured for dbh. These included 83 live trees and 40 snags, corresponding to a density of 332 and 160 trees per hectare, respectively. The size frequency distribution of live trees was right-skewed with a median of 56cm dbh, while that of the snags was reverse-J shaped with a median of 25cm dbh (Fig. 2.2b,c).

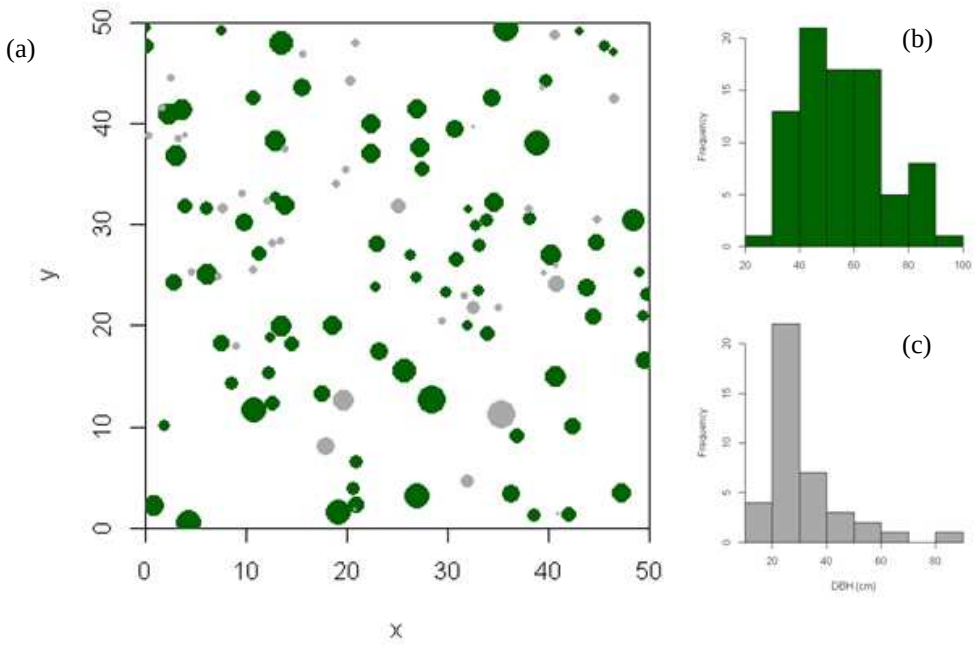

Fig. 2.2 Study plot characteristics: (a) Stem map showing live trees (green) and snags (grey) with the size of the circle proportional to dbh, and distributions of dbh for (b) live trees and (c) snags.

2.2.2 Light measurements

Stratified random sampling was used to select 10 sampling locations within the study plot. Hemispherical photographs were taken on a 5m grid covering the study area, then manually thresholded and analyzed using Gap Light Analyzer (Frazer et al., 1999) to obtain a preliminary

distribution of percent canopy openness. We split this distribution into three equal-sized strata, classified as “Low,” “Medium,” and “High” light groups (Fig. 2.3a). Three locations were chosen randomly from each strata, with the tenth location being that with the highest canopy openness value overall (Fig. 2.3b).

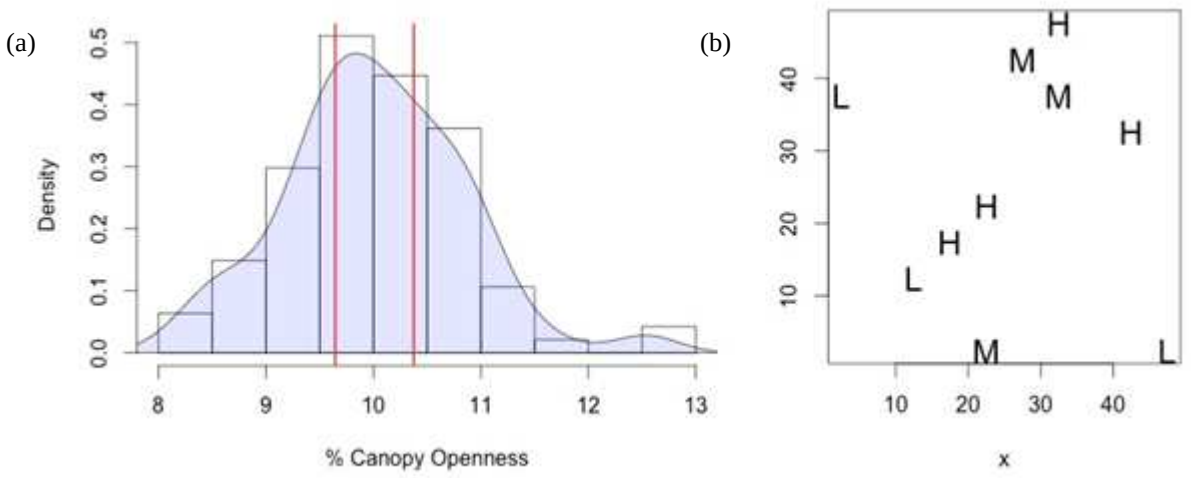

Fig. 2.3 Sampling locations within the study plot (b) were chosen randomly from Low, Medium and High strata based on the preliminary canopy openness distribution (a).

Light measurements were taken on a total of 15 days between July and September 2012, with one to three locations sampled each day such that each location was sampled at least twice. At dawn and dusk on each measurement day, hemispherical photographs were taken with a Nikon Coolpix 5000 digital camera in combination with a FC-E8 fisheye lens (Nikon Corporation, Tokyo, Japan). The camera was mounted on a tripod, horizontally leveled and oriented towards magnetic north. Photographs were taken at two heights, 1.5m and 1.9m above ground, in order to check the possible effect of height on light readings. Aperture was fixed at F5 following the recommendation of Zhang et al. (2005) and exposure bracketing accomplished by changing the shutter speed.

After taking the hemispherical photograph at dawn, a BF3 Sunshine Sensor (Delta-T Devices, Cambridge, UK) was mounted on a tripod at 1.5m above ground and stationed there until sunset. Over the course of the day, this BF3 sensor and its associated GP1 data-logger continuously logged below-canopy total and diffuse light readings at a rate of once per second. Meanwhile above-canopy light measurements were carried out similarly using another BF3 sensor in a nearby clearing. This open area was located approximately 1 km from our study site, with the BF3 mounted on a pole higher than any young trees in its 360º view to minimize obstruction of incoming solar radiation. Analysis of a hemispherical photograph on top of the pole estimated that only 4.89% of total light and 8.84% of diffuse light was obstructed at this location. Because this above-canopy reference site was relatively close to our study area, general cloud patterns could be expected to be similar and thus measurements were considered an acceptable estimation of the above-canopy light conditions for our study site (Ma, 2010).

2.2.3 BF3 daily integrative estimates

For each location-day we used BF3 readings above and below the canopy to calculate daily integrative estimates for total, diffuse and direct transmittance:

$$TransTotal_{day} = \frac{\sum_{day} Total\ PPFD\ Below}{\sum_{day} Total\ PPFD\ Above},$$

$$TransDiffuse_{day} = \frac{\sum_{day} Diffuse\ PPFD\ Below}{\sum_{day} Diffuse\ PPFD\ Above}, \quad (1)$$

$$TransDirect_{day} = \frac{\sum_{day} (Total - Diffuse)\ PPFD\ Below}{\sum_{day} (Total - Diffuse)\ PPFD\ Above},$$

where *day* is defined as the middle 80% of the time period between sunrise and sunset. We eliminated the data at the extremities because the overall light levels very early and late in the day are so low as to cause difficulties in dividing by above-canopy PPFD (see Fig. 2.4).

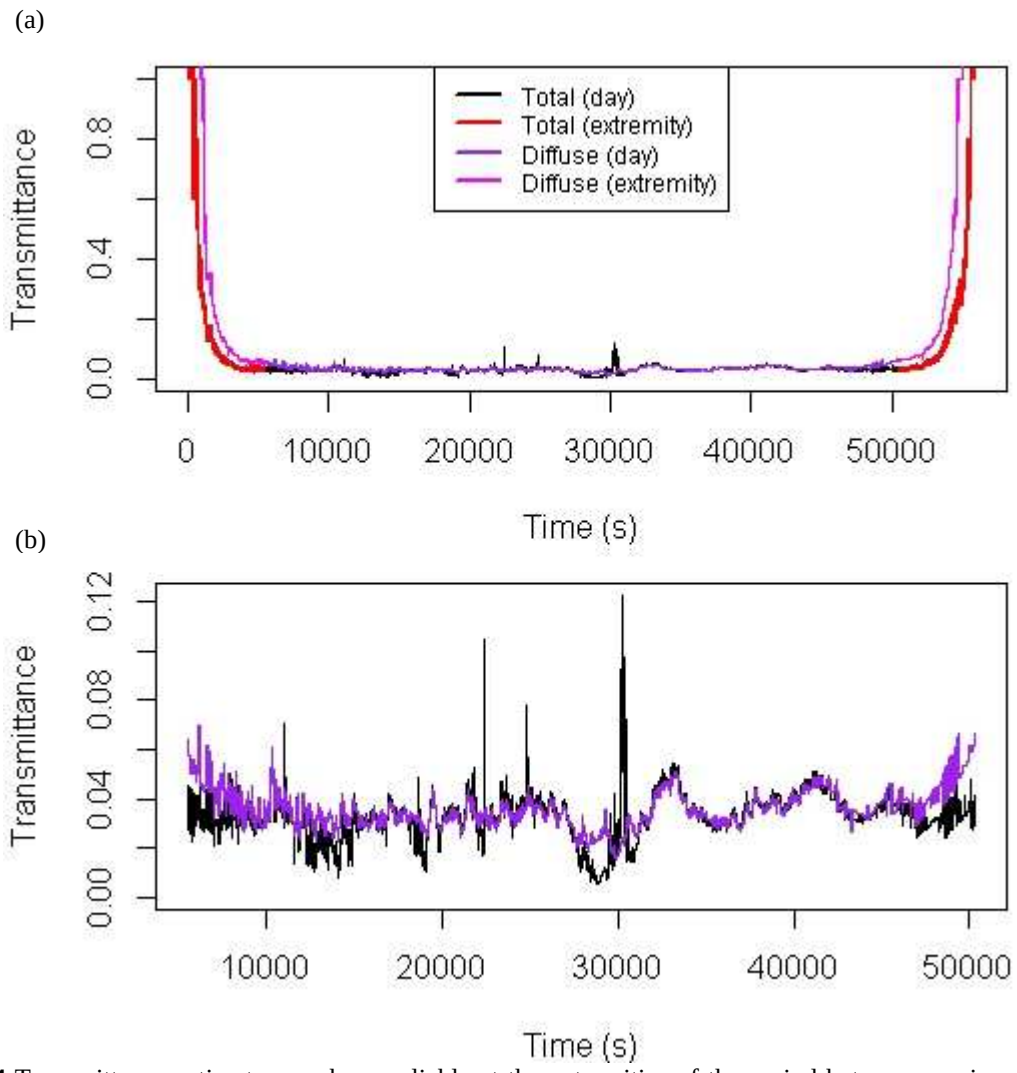

Fig. 2.4 Transmittance estimates can be unreliable at the extremities of the period between sunrise and sunset (a), thus we restricted daily BF3 readings to the middle 80% of this time period (b).

Hereafter we will treat the light intensities derived from direct BF3 measurements during the middle 80% of the day as 'reference' values, keeping in mind that a margin of error may be attached to these PAR measurements under field conditions (before transmittance calculations), due to spectral and cosine errors, and other technical limitations. The accuracy specifications for total PAR values are ±12% with a minimum accuracy of ±10 µmol/m²/s; the accuracy specifications for diffuse PAR values are ±15% with a minimum accuracy of ±10 µmol/m²/s (S. Williams, Delta-T Devices, personal communication).

2.2.4 Hemispherical image analysis (HIA)

For each set of exposure-bracketed photographs one exposure was chosen to optimize sky-foliage contrast, i.e. making the foliage appear dark but at the same time allowing the sky to appear white (Zhang et al., 2005). In addition, exposures were selected to be as consistent as possible between all samples (D. Sprugel, personal communication). Photographs taken at the same height as the BF3 readings (1.5m above ground) were used in the analysis; there was not a substantial difference in outputs calculated from photographs taken at different heights.

All of the digital images were converted to binary black (foliage) and white (sky) pixels via an automatic thresholding method based on edge detection (Nobis and Hunziker, 2005) using the software tool SideLook 1.1 (Nobis, 2005; Fig. 2.5). Thresholding is one of the most crucial and uncertain steps in HIA and there has been much interest in developing objective, automatic, operator-independent thresholding methods (Cescatti, 2007; Jonckheere et al., 2005). Manual thresholding has often been criticized as subjective and a major source of error, but the edge detection approach is objective and reproducible. Nobis and Hunziker (2005) showed that the automatic threshold algorithm in SideLook improved precision and correspondence with direct measurements, especially in comparison with single manual thresholding.

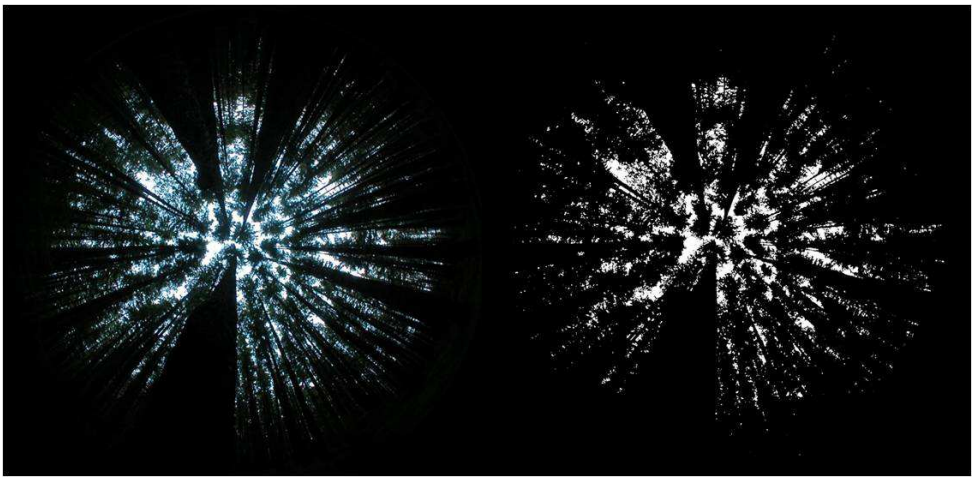

Fig. 2.5 A digital hemispherical photograph before (left) and after (right) automatic thresholding with SideLook.

The thresholded images were then processed through the software Gap Light Analyzer (GLA) Version 2.0 (Frazer et al., 1999) and transmittance calculated for direct, diffuse, and total light. Direct transmittance values are obtained by tracking the solar path through the pixels given latitude, growing season, and various other user-defined parameters (Fig. 2.6). The simplified radiation model within GLA assumes that when the sun position is obstructed by the canopy direct radiation is zero, and when unobstructed direct radiation is equal to the above-canopy value. Beam enrichment by scattered and reflected radiation is not considered (Hardy et al., 2004). Total transmittance is the proportion equivalent to the gap light index (GLI) developed by Canham (1988), which is just a weighted sum of diffuse and direct transmittance:

$$GLI = T_{total} = \left(T_{diffuse} P_{diffuse}\right) + \left(T_{direct} P_{direct}\right), \quad (2)$$

where $P_{diffuse}$ and $P_{direct} = 1 - P_{diffuse}$ are the proportions of above-canopy incident radiation received as diffuse sky radiation and direct beam radiation, respectively, while $T_{diffuse}$ and T_{direct} are the proportions of diffuse and direct radiation that are transmitted to the understory (Canham, 1988). P_{direct} is also known as the 'beam fraction' parameter within GLA, and defaults to 0.5 in absence of external measurements.

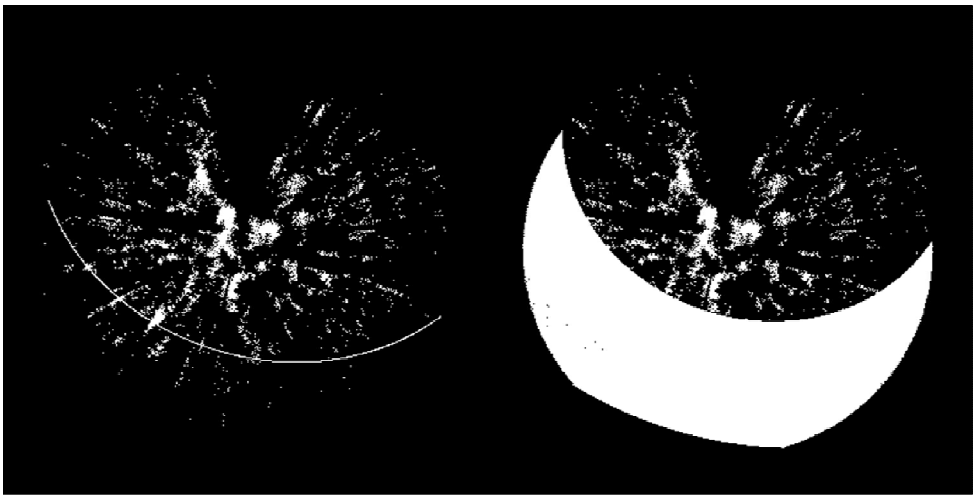

Fig. 2.6 Solar path calculated by GLA for location L3 on Aug 31 (left) and for the growing season (right).

Region-specific model parameters (Table 2.2) used to derive above-canopy solar radiation data were based on the best available estimates as recommended by the GLA Users Manual. The solar constant is the total radiant flux of the sun on a perpendicular surface located outside the earth's atmosphere at the mean distance of 1 astronomical unit. The cloudiness index is the ratio of global radiation incident on a horizontal surface at the ground to the amount of extraterrestrial radiation incident on a horizontal surface outside the earth's atmosphere. The spectral fraction is the fraction of global solar radiation (0.25µm to 25.0 µm) incident on a horizontal surface at the ground that falls within a limited range of the electromagnetic spectrum (in this case 400 to 700 nm). The beam fraction is the ratio of direct (beam) to total (global) spectral radiation incident on a horizontal surface at the ground over a specified period. The clear-sky transmission coefficient is a factor that describes the regional clarity of the atmosphere with respect to the instantaneous transmission of direct (beam) radiation (Frazer et al., 1999). A uniform overcast (UOC) sky model was chosen to describe the light intensity of the diffuse sky. The images were divided into 36 azimuth and 9 zenith regions. Two time frames were employed to analyze each image: a growing season from March 1 to November 30 as well as the one specific date the photograph was taken, in order to obtain a daily transmittance estimate comparable to that calculated from the BF3 readings.

Parameter	**Value**
Solar constant (W/m²)	1367
Cloudiness index	0.55
Spectral fraction	0.45
Beam fraction	0.5
Clear-sky transmission coefficient	0.65

Table 2.2 Values of region-specific model parameters used in GLA.

2.2.5 BF3 instantaneous estimates

Following the idea introduced by Parent and Messier (1996) for quantum sensors, of using an instantaneous estimate of understory light availability to save sampling effort, previous studies employing the BF-series sensors have used instantaneous readings above and below the canopy to estimate the transmittance (e.g. Paquette et al., 2007; D'orangeville et al., 2011; Cogliastro and Paquette, 2012). Since continuous sampling over the course of the day may be costly and time-consuming, we decided to investigate whether instantaneous estimates could indeed be a reasonable alternative. We derived instantaneous estimates from the daily BF3 readings using two sub-sampling methods. In the first method, an instantaneous reading was selected at solar noon (SN, defined as the midpoint between sunrise and sunset) from both above-canopy and below-canopy time series:

$$TransTotal_{SN} = \frac{Total\ PPFD\ Below_{SN}}{Total\ PPFD\ Above_{SN}},$$

$$TransDiffuse_{SN} = \frac{Diffuse\ PPFD\ Below_{SN}}{Diffuse\ PPFD\ Above_{SN}} \quad (3)$$

In the second method, a 10-minute window was randomly selected from each of the four hours around solar noon and used to calculate an average transmittance:

$$TransTotal_{10min} = \frac{mean(Total\ PPFD\ Below_{10min})}{mean(Total\ PPFD\ Above_{10min})},$$

$$TransDiffuse_{10min} = \frac{mean(Diffuse\ PPFD\ Below_{10min})}{mean(Diffuse\ PPFD\ Above_{10min})} \quad (4)$$

The median of these four 10-minute averages was also calculated for each location on each day.

These sub-sampling methods are illustrated in Fig. 2.7. In some cases the instantaneous reading at solar noon happened to fall on a sunfleck (e.g. Fig. 2.7a,b), thus giving an inflated estimate for the overall transmittance, while in other cases it fell on a local minimum (e.g. Fig. 2.7c) or somewhere in between (e.g. Fig. 2.7d). The 10-minute means tended to capture more of the average behavior.

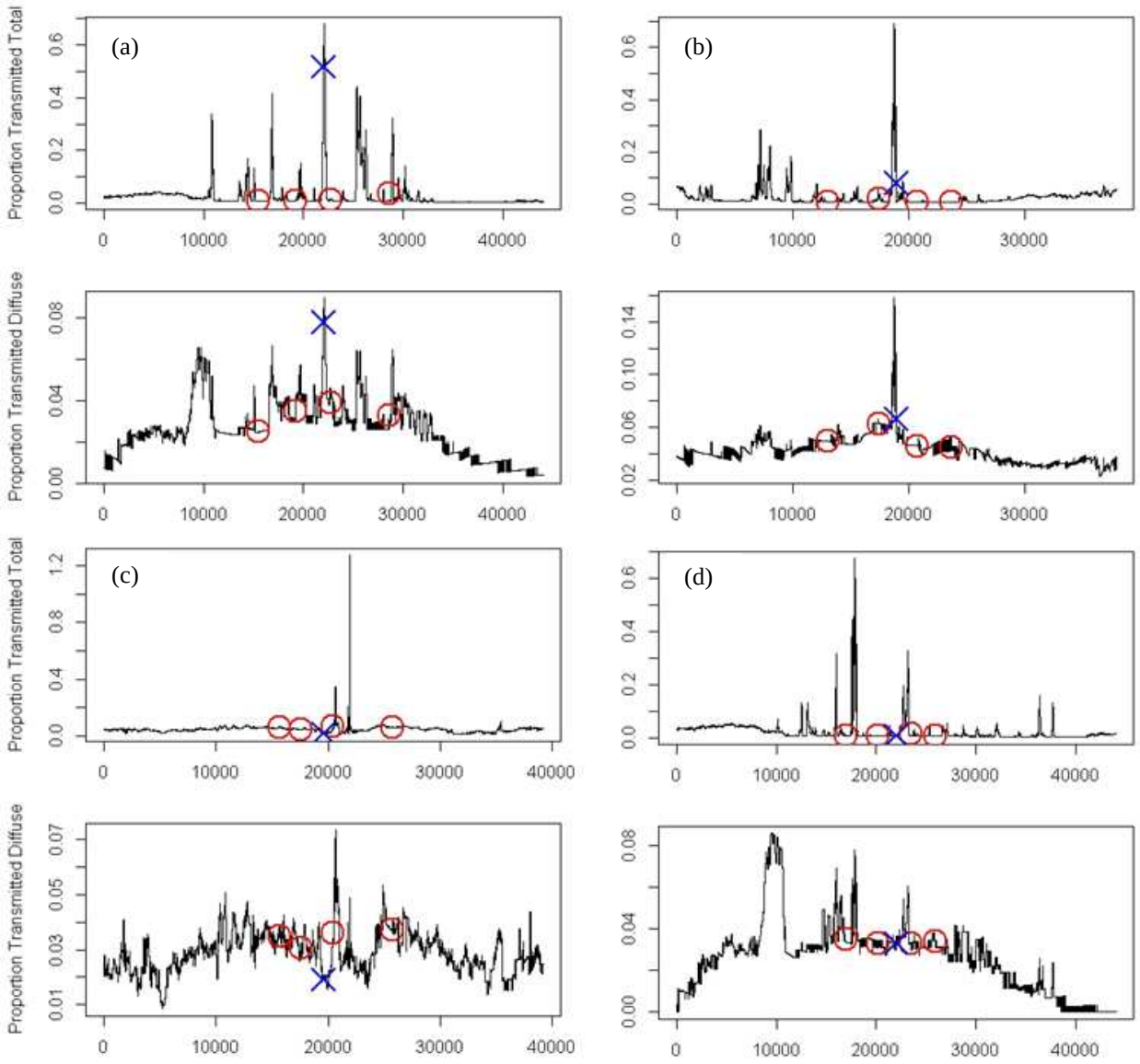

Fig. 2.7 Instantaneous readings selected from daily continuous BF3 readings on four different days. For each day the top graph shows total transmittance while the bottom graph shows diffuse transmittance. Blue X's indicate the instantaneous reading at solar noon, while red O's indicate locations of 10-minute means taken around solar noon.

2.3 Results

2.3.1 Comparison of daily integrative BF3 vs. HIA

Daily integrative BF3 estimates of diffuse transmittance ranged from 1.13% to 4.42% of above-canopy light, compared to 4.24% to 9.82% estimated by HIA. Mean diffuse transmittance for each location is reported in Table 2.3. In HIA, diffuse transmittance is derived solely based on the proportion of white (sky) pixels observed and the diffuse radiation model parameters and does not depend on the solar path. Thus it is the same according to GLA for a single day as for the growing season. There was not a significant correlation between the diffuse transmittance estimates obtained from the two methods (see Table 2.5, page 26), and HIA consistently overestimated the diffuse transmittance relative to the BF3 (Fig. 2.8). The variation in HIA estimates for each location is mainly due to differences in image exposures, while the variation in BF3 estimates for each location results mainly from differences in daily weather patterns.

HIA estimates for total transmittance depended on the time frame applied, since their calculation included direct transmittance which utilized modeled solar paths. Total transmittance from HIA for the growing season ranged from 3.22% to 8.05% of above-canopy light, compared to 2.73% to 9.17% for single-day estimates. In contrast, the daily integrative BF3 estimates of total transmittance ranged from 0.054% to 4.97% of above-canopy light. BF3 total estimates were not significantly correlated with either of the HIA total estimates. In both cases, HIA overestimated total transmittance on average relative to the BF3 (Fig. 2.9a,b).

Daily integrative BF3 estimates for direct transmittance were sometimes inaccurate, especially on overcast days. On overcast days total light is composed almost entirely of diffuse light, so subtracting to find “direct” radiation is inadvisable. The intrinsic margin of error of the

BF3 instrument may have a larger influence on the calculated proportions on these days. The BF3 direct estimates were not significantly correlated with either of the HIA direct estimates. Looking only at days classified as having "Mostly Clear" skies, the relationship between BF3 and HIA (both growing season and single-day) direct estimates was consistent with the results for total and diffuse transmittance (Fig. 2.9c,d).

Location	HIA_{day}	$BF3_{day}$
L1	0.0620 (0.0066)	0.0267 (0.0134)
L2	0.0586 (0.0086)	0.0288 (0.0004)
L3	0.0622 (0.0116)	0.0370 (0.0079)
M1	0.0796 (0.0151)	0.0404 (0.0007)
M2	0.0521 (0.0089)	0.0291 (0.0117)
M3	0.0669 (0.0080)	0.0354 (0.0124)
H1	0.0628 (0.0058)	0.0305 (0.0086)
H2	0.0742 (0.0094)	0.0335 (0.0051)
H3	0.0612 (0.0111)	0.0185 (0.0059)
H4	0.0787 (0.0082)	0.0248 (0.0031)

Table 2.3 Mean diffuse transmittance as estimated by HIA (including both dawn and dusk photographs) and BF3 for each sampling location. Standard deviations are in parentheses.

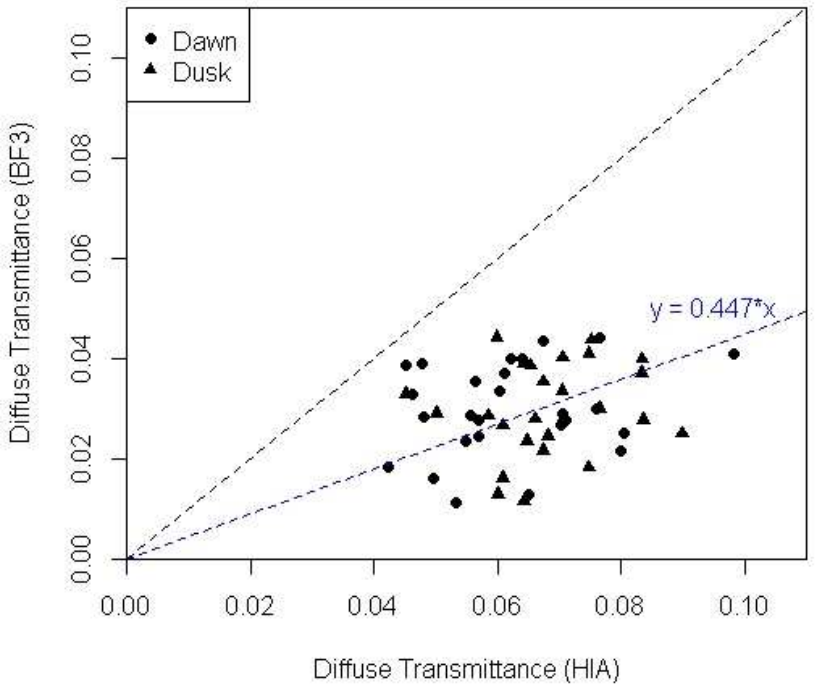

Fig. 2.8 Daily integrative BF3 estimates compared to HIA estimates of diffuse transmittance. The OLS regression line through the origin (blue dashed line) is shown solely for visual reference.

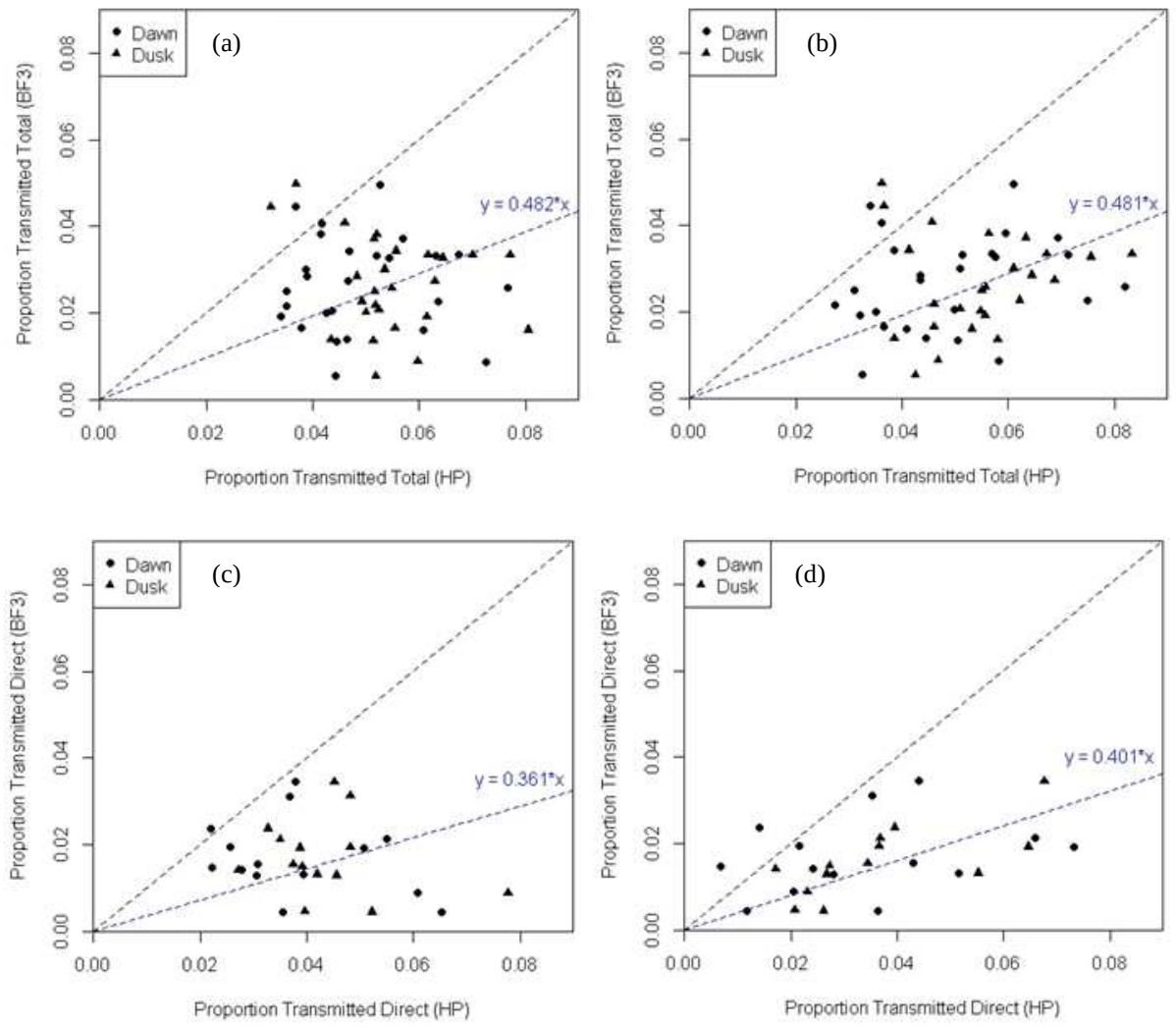

Fig. 2.9 Daily integrative BF3 estimates compared to HIA estimates of total transmittance (a, growing season; b, single day) and direct transmittance (c, growing season; d, single day).

The HIA estimates of total transmittance can be adjusted by setting the beam fraction within GLA, i.e. P_{direct} in Eqn. (1), to reflect daily radiation patterns as measured by the BF3. Beam fraction is largely a function of cloud cover – on a clear day most of the incident total daily solar radiation is received as direct (beam) radiation, compared to an overcast day when most of the total daily solar radiation is received as diffuse radiation. The beam fraction can easily be estimated from the daily above-canopy BF3 readings:

$$P_{diffuse} = \frac{\sum_{day} Diffuse\ PPFD\ Above}{\sum_{day} Total\ PPFD\ Above},$$

$$P_{direct} = 1 - P_{diffuse} \quad (5)$$

On clear days the beam fraction is greater than 50% (Table 2.4), so direct transmittance is weighted more heavily in the total transmittance calculation. On overcast days the reverse occurs. Since HIA estimates of direct transmittance tended to be lower in general than diffuse transmittance, this weight adjustment tended to pull the total transmittance toward lower values for clear days and toward higher values for overcast days (Fig. 2.10). Weight-adjusted single-day estimates were significantly but not strongly correlated with daily integrative BF3 estimates (see Table 2.5, page 26).

Weather	Above-canopy	Understory
Mostly clear	0.781	0.655
Variable	0.394	0.382
Overcast	0.084	0.334

Table 2.4 Mean proportion of direct light out of total light for above-canopy (beam fraction) and understory.

Regression outputs are summarized in Table 2.6 (page 26). In this study regression analysis was used simply as a tool to describe linear relationships among variables, and daily integrative BF3 estimates were set as the independent variable for consistency as well as to allow prediction of daily integrative BF3 estimates from indirect estimates. Weight-adjusted single-day HIA estimates of total transmittance performed the best out of all the HIA estimates, with an r^2 value of 0.25.

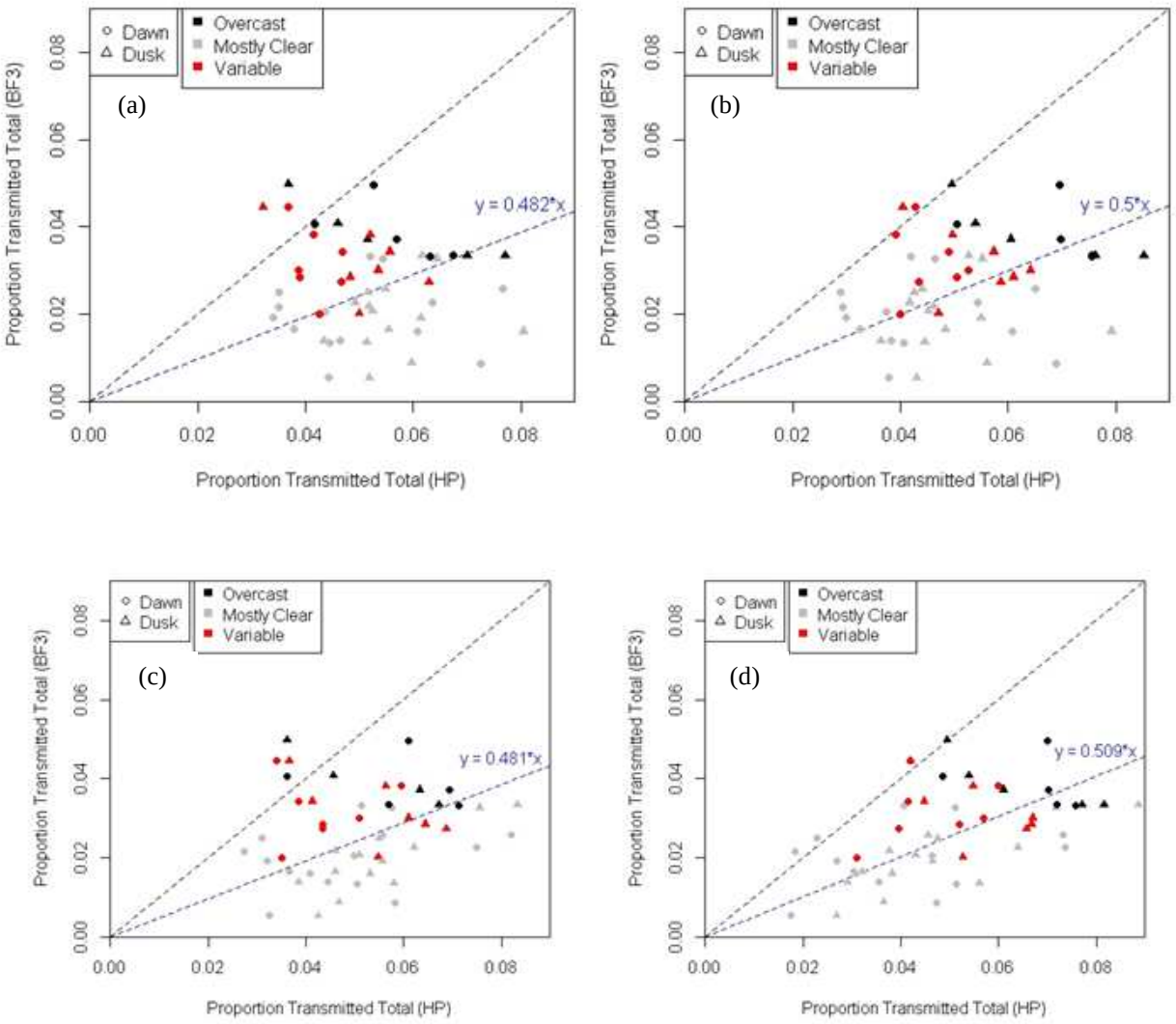

Fig. 2.10 Daily integrative BF3 estimates compared to HIA estimates of total transmittance for growing season (a, without weight adjustment; b with weight adjustment) and single day (c, without weight adjustment; d, with weight adjustment). The weight adjustment tended to lower values on clear days and increase values on cloudier days.

2.3.2 Comparison of daily integrative BF3 vs. instantaneous BF3

The instantaneous estimate of diffuse transmittance at solar noon ($TransDiffuse_{SN}$) was correlated with the daily integrative estimate ($TransDiffuse_{day}$), though subject to outliers. In 10 out of 26 location-days, $TransDiffuse_{SN}$ was greater than the third quartile of instantaneous diffuse transmittance over the course of the day, indicating that solar noon fell upon a local maximum (Fig. 2.11a). In 13 out of 14 cases where $TransDiffuse_{SN}$ overestimated $TransDiffuse_{day}$ the weather had been classified as "Mostly Clear," while in 11 out of 12 cases where $TransDiffuse_{SN}$ underestimated $TransDiffuse_{day}$ the weather had been classified as either "Overcast" or "Variable."

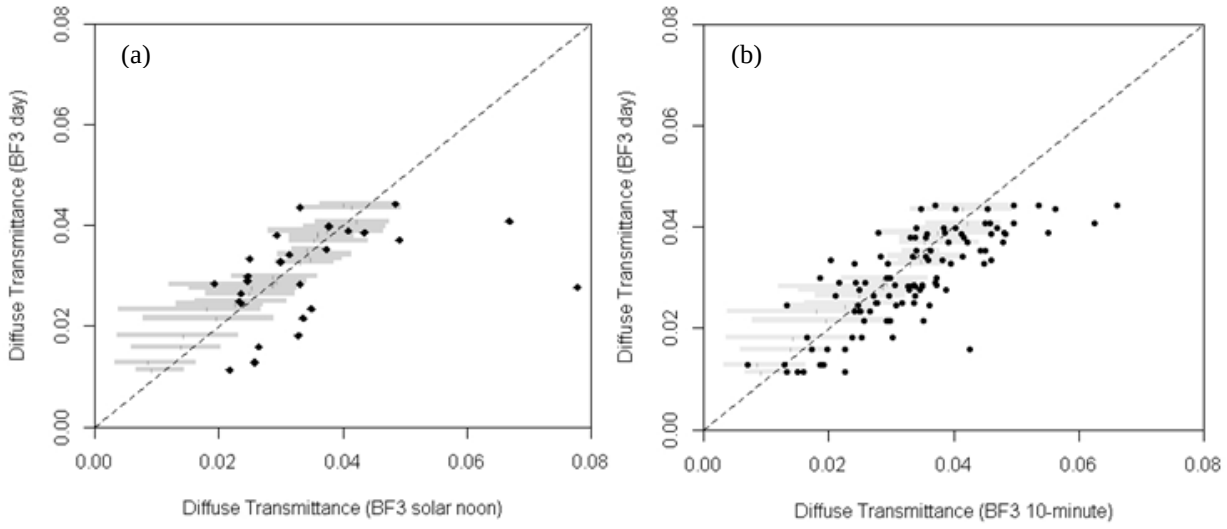

Fig. 2.11 Daily integrative BF3 estimates of diffuse transmittance compared to (a) instantaneous BF3 estimates at solar noon and (b) randomly selected 10-minute means within two hours of solar noon. Gray bars represent the interquartile range of diffuse transmittance values for each day.

The 10-minute means clustered more strongly around the identity line, though with considerable variation (Fig. 2.11b). The median of the four 10-minute means for each location-day was strongly correlated with the daily integrative estimate and was much closer to a 1:1 relationship (Fig. 2.12). Based on these results we might recommend that a researcher wishing to

minimize sampling effort with a BF-series sensor use the median of several 10-minute means within two hours of solar noon as a proxy for daily diffuse transmittance. This is convenient since most data loggers give the option to record 10-minute means, and a single sensor could be moved to multiple locations in the understory. In our particular case, with an r^2 of 0.88,

$$TransDiffuse = 0.9245\left(median\left(TransDiffuse_{10min}\right)\right) - 0.0008 \quad (6)$$

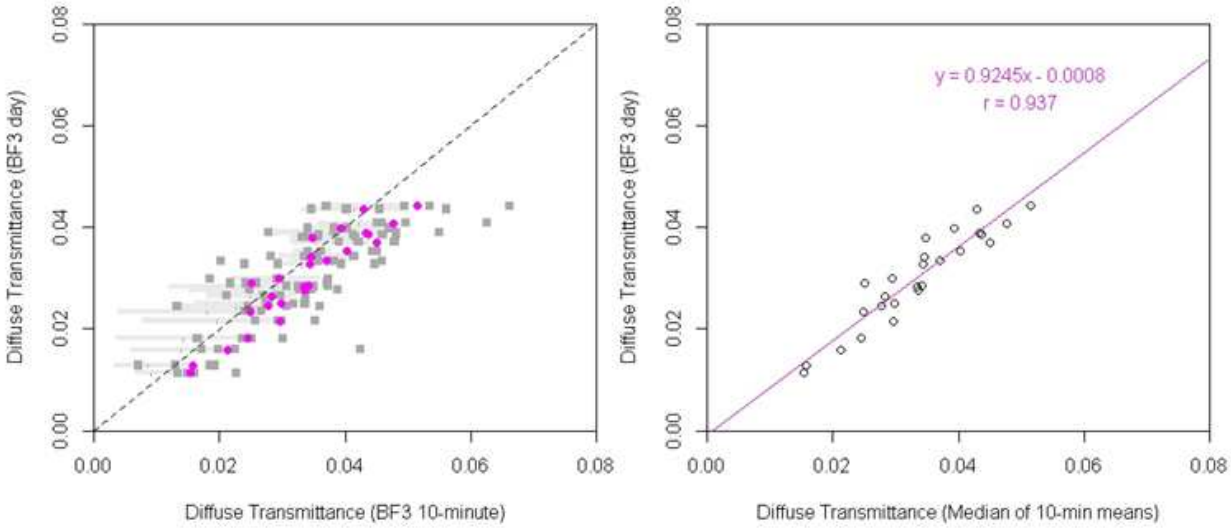

Fig. 2.12 Daily integrative BF3 estimates of diffuse transmittance compared to the median of 10-minute means.

There was not a significant correlation between the instantaneous estimate of total transmittance at solar noon ($TransTotal_{SN}$) and the daily integrative estimate ($TransTotal_{day}$). In the majority of cases, $TransTotal_{SN}$ underestimated $TransTotal_{day}$ (Fig. 2.13b). However, there were some outliers including an extreme outlier at location H4 on July 25, 2012 (a "Mostly Clear" day), where the instantaneous transmittance at solar noon was greater than 0.5, about an order of magnitude greater than the maximum daily estimate for all location-days (Fig. 2.13a). This points to the dangers of using a single reading to approximate understory light availability over a longer time period. The 10-minute means also exhibited some outliers though none as

extreme as for solar noon. The median of the four 10-minute means for each location-day was significantly correlated with the daily integrative estimate but the relationship was not as strong as for diffuse transmittance (Fig. 2.13d). In our particular case, with an r^2 of 0.61,

$$TransTotal = 0.5525\left(median\left(TransTotal_{10min}\right)\right) + 0.0127 \quad (7)$$

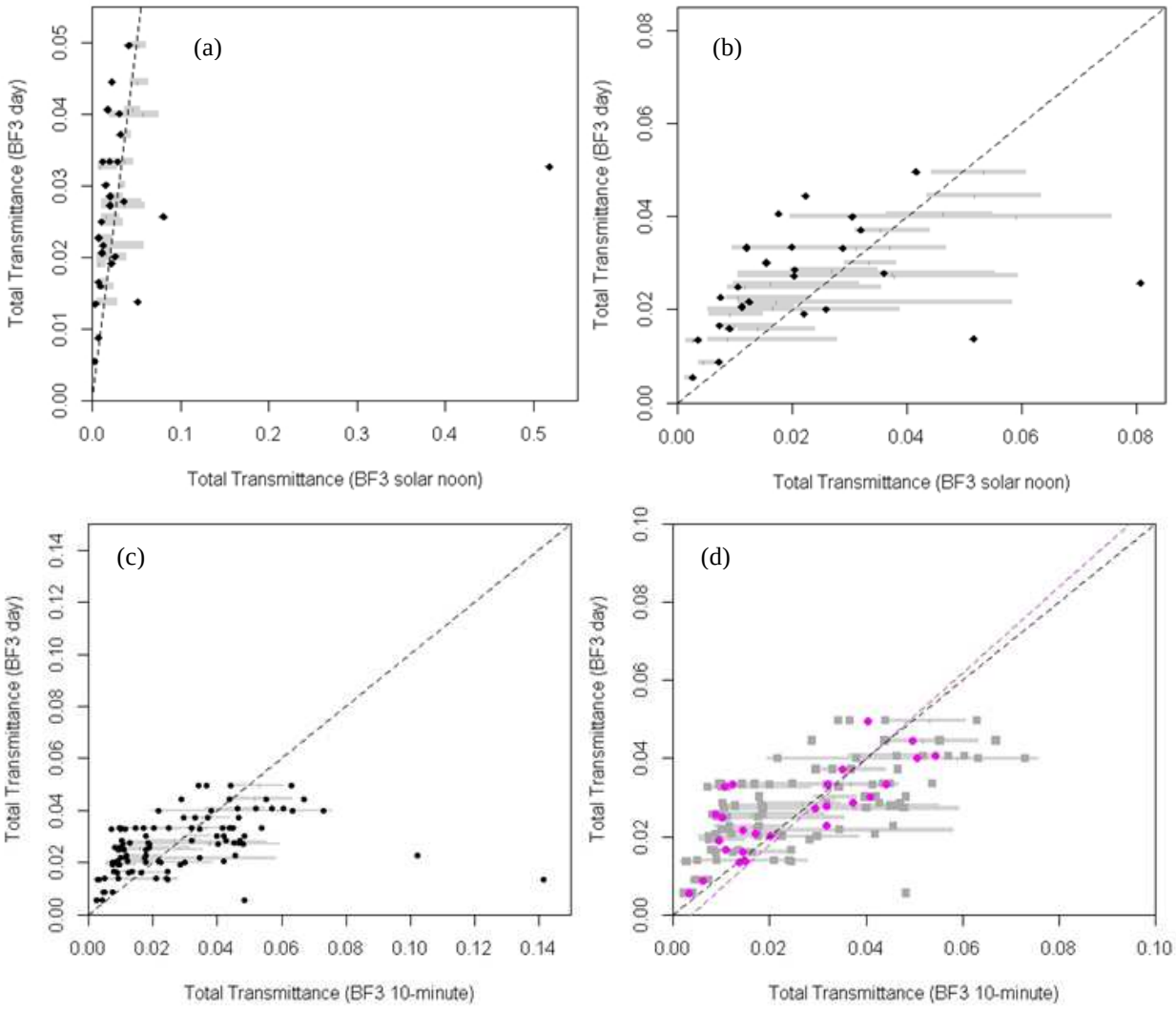

Fig. 2.13 Daily integrative BF3 estimates for total transmittance compared to instantaneous BF3 readings at solar noon (a; b, shown without the most extreme outlier) and (c) randomly selected 10-minute means around solar noon. The median of 10-minute means for each day are the magenta points in (d).

Diffuse	$HIA_{GS} = HIA_{day}$	$BF3_{SN}$	$_{med}BF3_{10min}$
$BF3_{day}$	0.188; 0.169	0.421*; 0.537**	0.937**; 0.930**
$HIA_{GS} = HIA_{day}$		0.327*; 0.182	0.211; 0.177
$BF3_{SN}$			0.561**; 0.637**
$_{med}BF3_{10min}$			

Total	HIA_{GS}	HIA_{day}	$HIA_{GS.wt}$	$HIA_{day.wt}$	$BF3_{SN}$	$_{med}BF3_{10min}$
$BF3_{day}$	-0.126; -0.054	0.186; 0.204	0.264; 0.315*	0.499**; 0.522**	0.170; 0.536**	0.780**; 0.743**
HIA_{GS}		0.714**; 0.728**	0.800**; 0.0773**	0.523**; 0.493**	0.140; 0.008	-0.155; -0.170
HIA_{day}			0.635**; 0.647**	0.878**; 0.863**	0.226; 0.188	0.014; 0.030
$HIA_{GS.wt}$				0.669**; 0.662**	0.119; 0.158	0.336*; 0.314*
$HIA_{day.wt}$					0.166; 0.294*	0.403**; 0.412**
$BF3_{SN}$						-0.16; 0.316
$_{med}BF3_{10min}$						

Table 2.5 Pearson product-moment and Spearman rank correlation coefficients between all pairs of transmittance estimates. The former is a measure of the linear correlation between variables, while the latter assesses strength of monotonic relationship and is less sensitive to outliers.

Y	X	Intercept	Slope	r^2	RMSE	n
$BF3_{day}$ (Diffuse)	$HIA_{GS} = HIA_{day}$	0.0206	0.1420	0.0354	0.0091	52
	$BF3_{SN}$	0.0203	0.2818	0.1776	0.0085	26
	$_{med}BF3_{10min}$	-0.0008	0.9245	0.8775	0.0033	26
$BF3_{day}$ (Total)	HIA_{GS}	0.0327	-0.1179	0.0159	0.0110	52
	HIA_{day}	0.0193	0.1387	0.0347	0.0108	52
	$HIA_{GS.wt}$	0.0156	0.2145	0.0699	0.0106	52
	$HIA_{day.wt}$	0.0107	0.3169	0.2486	0.0096	52
	$BF3_{SN}$	0.0257	0.0189	0.0288	0.0111	26
	$_{med}BF3_{10min}$	0.0127	0.5525	0.6087	0.0070	26

Table 2.6 Outputs from linear regression with daily integrative BF3 estimates of diffuse and total transmittance as the independent variables. These relationships correspond to the yellow-highlighted boxes in Table 2.5.

2.3.3 Sunflecks

One of the benefits of directly measuring light with a light sensor such as the BF3 over an extended period of time is that it can provide a complete rendition of the complex light microclimate at a given location, including the frequency, intensity and duration of direct light events (sunflecks) allowed into the understory through gaps in the canopy (Gendron et al., 1998). Although sunflecks are generally brief in duration, lasting from a few seconds to a few minutes, they are thought to contribute substantially to total understory light available for photosynthesis in a variety of forest communities (Chazdon, 1988; Way and Pearcy, 2012). On clear days, 10-85% of daily PPFD may be contributed by sunflecks, and sunflecks have been linked to carbon gain in understory plants (Chazdon and Pearcy, 1991).

Although sunflecks have been a research interest for decades, a precise quantitative definition of the term 'sunfleck' has not been developed (Smith and Berry, 2013). Qualitatively, sunflecks can be distinguished as pulses of predominantly direct light in contrast to background levels of diffuse light. Thus sunflecks have typically been defined by a somewhat arbitrary choice of threshold value based on the perceived background diffuse light level. This threshold necessarily varies between forest types (see Table 2.7), and different choices of threshold result in different estimates of the contribution of sunflecks, making it difficult to distinguish between the effects of different thresholds and real differences in sunfleck contribution (Lieffers et al., 1999). Another difficulty, particularly in tall forests with dense canopies, is the high frequency of sunflecks generated by penumbral effects. These penumbral sunflecks contain a relatively high proportion of diffuse light, and may reach peak intensity only slightly higher than background diffuse light (Chazdon and Pearcy, 1991).

Study	Habitat type	Sunfleck threshold (µmol/m²/s)	Sampling rate	Sampling duration	Sunfleck contribution to total light (%)
Chen and Klinka 1997	Douglas-fir, Pacific Northwest	50	12 readings per second	<18 days	32
Messier and Puttonen 1995	Mature Scots pine, Finland	90 or 175 depending on the stand	5-min averages	4-6 days	90 (20-yr-old stands)
	Open 7-year-old Scots pine	350			65
Lei and Lechowicz 1990	Eastern deciduous	100	Not reported	Samples over 16 days	53
Messier et al. 1998	Boreal forests of eastern Canada	100	One 5-sec average per minute	One full sunny day	59-86, depending on species
	Mixed boreal forests of Quebec	250			28-57, depending on species
Lei et al. 2006	Eastern deciduous	10	Ten 1-min averages over a 10-min period	7 days	42-92 on clear days; 67-71 on overcast days
	Rhododendron thickets				0-8
Brantley and Young 2009	Shrub thickets	25	Every second for ~15min, midday	Several cloudless days	5
	Pine forest	50			31
	Deciduous forest	100			22
Vierling and Wessman 2000	Congolese rain forest (3m height)	100	Every 1.5 seconds	12 days	0-22, depending on the day

Table 2.7 Sunfleck thresholds, sampling methods and estimated sunfleck contribution for a range of forest types.

We explored several quantitative definitions of sunfleck occurrence using our daily BF3 readings taken at 1-second intervals over 80% of the period between sunrise and sunset. The first definition (definition A) set a threshold value of 50 µmol/m²/s (e.g. Fig. 2.14a,c). This followed the threshold set by Chen and Klinka (1997) for a similar forest environment, and corresponded closely to the BF3 sensor's internal sunshine state indicator. We also investigated the definition by Ma (2010) of a sunfleck as whenever the total light intensity is greater than four times the diffuse light intensity. Ma's definition missed some peaks that occurred with higher diffuse readings, and tended to give false positives when diffuse levels were very low (e.g. Fig. 2.14b,d).

The definition of sunflecks used by most studies (e.g. Table 2.7) applies a constant threshold and ignores differences in background light levels between days. To account for these differences, we established a new definition (definition B) in which sunflecks occur when the

direct (difference between total and diffuse) light intensity is greater than the daily mean total light intensity. Using the daily mean total light as a threshold for direct light values appeared to give visually superior results compared to the previous definitions. It picked up more of the low-intensity sunflecks that were missed by setting a constant threshold (Fig. 2.15), and may thus provide a more accurate depiction of the temporal dynamics of understory light. However, it is not clear how much these low-intensity sunflecks contribute to photosynthesis in understory plants. Sunflecks that are low in intensity also tend to be short in duration, and their utilization may be limited by photosynthetic induction requirements. On the other hand, frequent low-intensity sunflecks might assist in maintaining a background level of induction during the day.

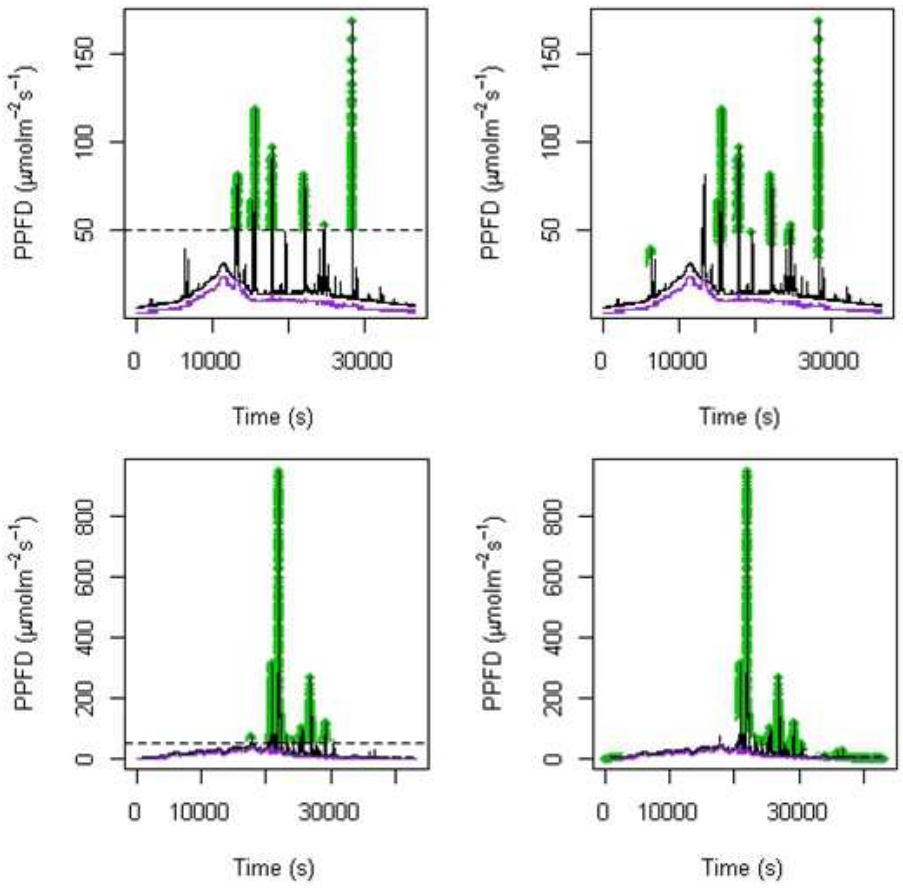

Fig. 2.14 Sunflecks (green) identified by definition A (left) and as defined by Ma (2010) (right). Top: Site H2 on September 13, 2012; Bottom: Site H1 on July 31, 2012.

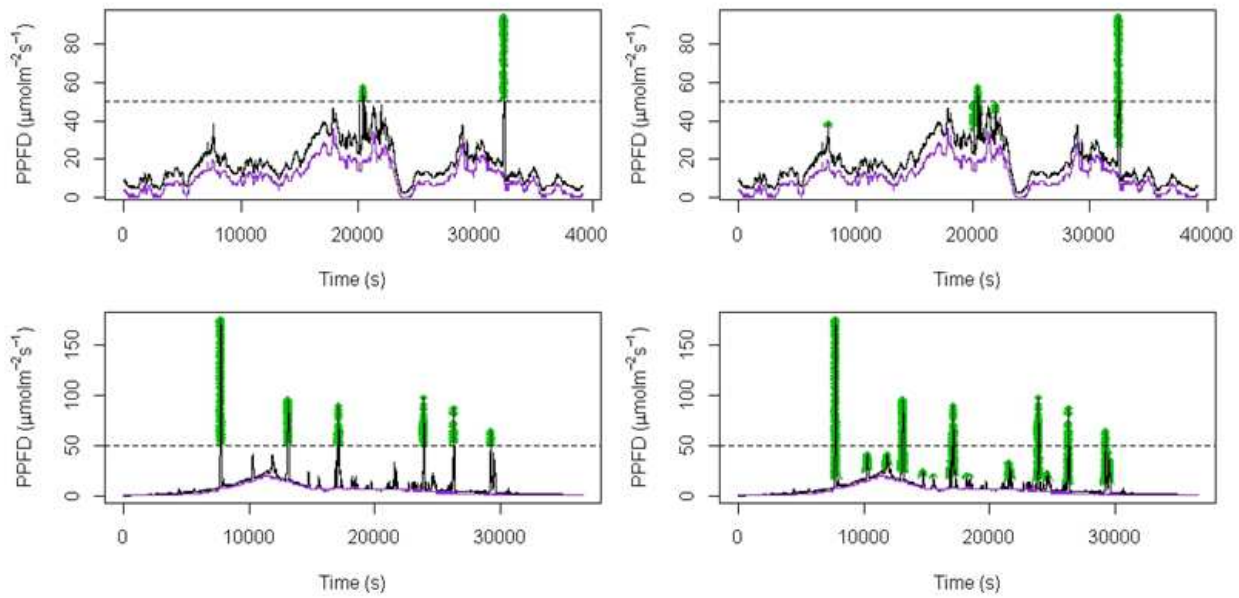

Fig. 2.15 Sunflecks (green) identified by definition A (left) and definition B (right). Top: Site H4 on August 28, 2012; Bottom: the same site on September 13, 2012

We calculated the percentage of daily total light contributed by sunflecks using both definitions A and B. Sunflecks contributed a greater proportion (almost 50%) of total light on clear days than on days with more cloud cover (Table 2.8). Mean sunfleck contribution grouped by weather did not differ widely between the two definitions, likely because the inclusion of low-intensity sunflecks did not add much to the sum of PPFD during sunflecks. Sunfleck contribution was lower according to definition B for the "Variable" weather group due to the particular dynamics observed on July 18, 2012, namely the presence of total light readings greater than 50 µmol/m²/s but not much greater than the concurrent diffuse light readings (see Fig. 2.16).

Weather	% Sunfleck contribution (Definition A)	% Sunfleck contribution (Definition B)
Mostly clear	41.27	49.85
Variable	19.67	15.06
Overcast	2.40	2.70

Table 2.8 Mean percentage of daily total light contributed by sunflecks identified by definitions A and B under different weather conditions.

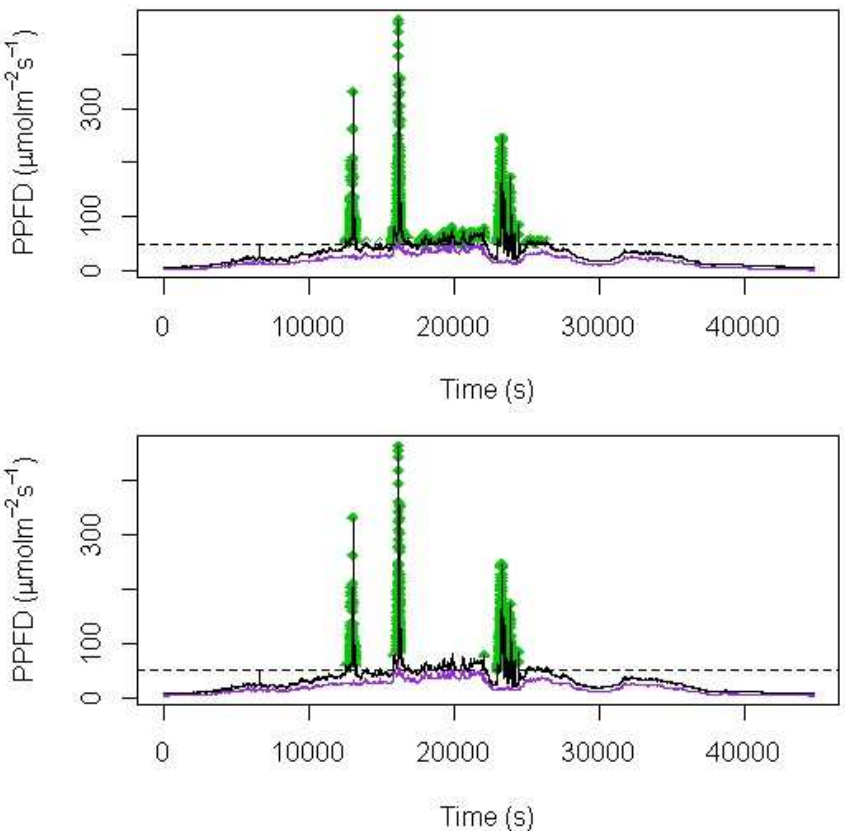

Fig. 2.16 Sunflecks (green) identified by definition A (top) and definition B (bottom) for site M2 on July 18, 2012. Definition A counted some total light readings as sunflecks that were not much higher than concurrent diffuse light readings.

Important considerations for carbon gain during sunflecks include duration, frequency and peak intensity of sunflecks (Chazdon and Pearcy, 1991). By applying run length encoding to the BF3 readings we were able to extract duration and peak intensity for sunflecks according to both definitions A and B. Distributions across all samples were heavily skewed toward lower values (Fig. 2.17). Under definition A around 85% of sunflecks lasted for less than 1 minute, and 93% of those lasted for less than 30 seconds. About 84% of sunflecks peaked at less than 100 µmol/m²/s PPFD, with almost half of those being between 50-55 µmol/m²/s PPFD. Under definition B around 84% of sunflecks lasted for less than 1 minute, and 96% of those lasted for less than 30 seconds. Over 89% of sunflecks peaked at less than 100 µmol/m²/s PPFD, with almost 65% of those being under 50 µmol/m²/s PPFD. More than half of all sunflecks under

definition B would have been overlooked by definition A because they were below the 50 µmol/m²/s threshold. Bivariate histograms of sunfleck duration and peak intensity show that the vast majority of sunflecks occurring in our understory environment were both short in duration and low in intensity, although there was a wide range of experienced values (see Fig. 2.18).

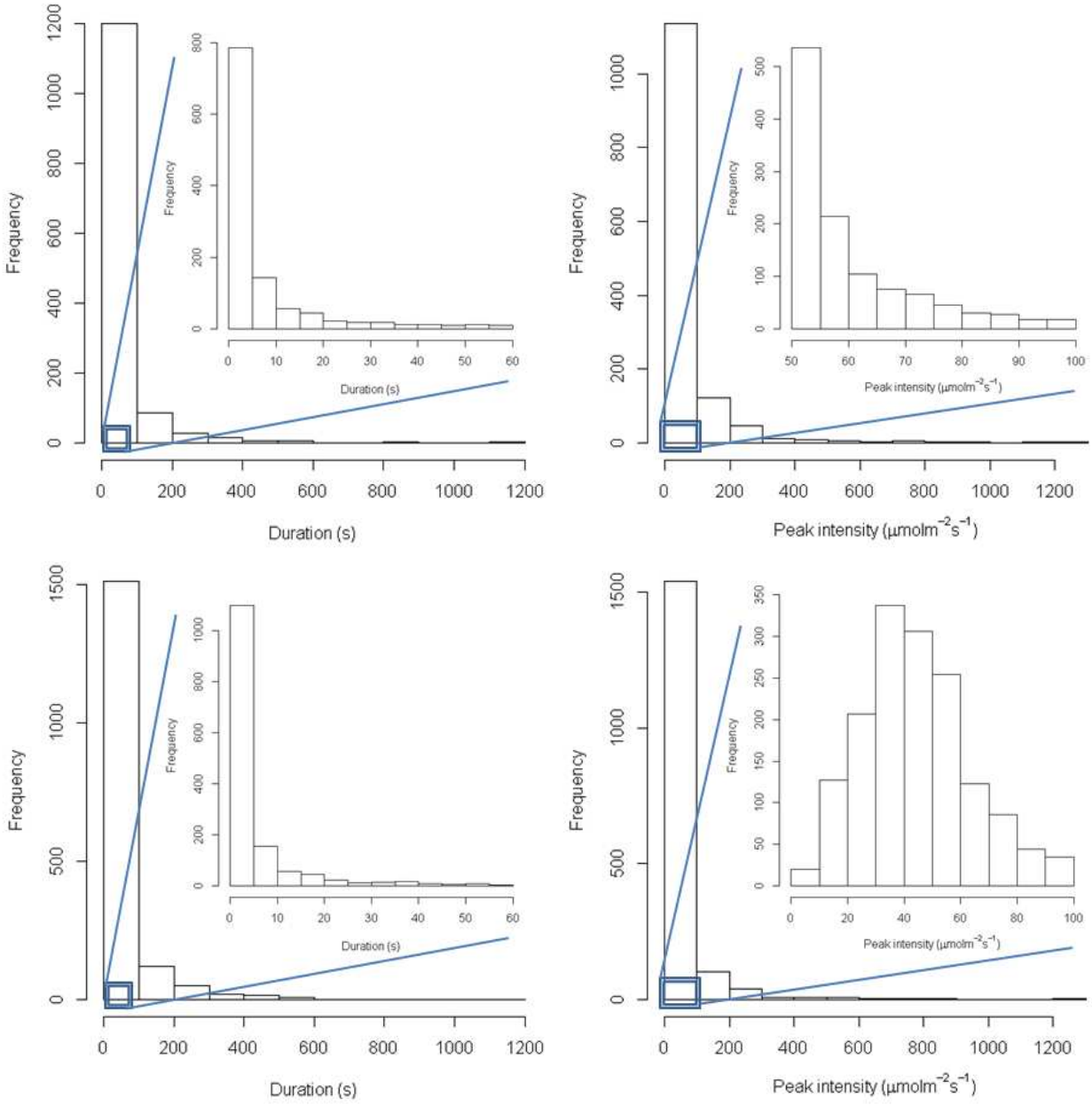

Fig. 2.17 Distribution of sunfleck duration (left) and peak intensity (right) across all samples, with sunflecks identified by definition A (top) and definition B (bottom).

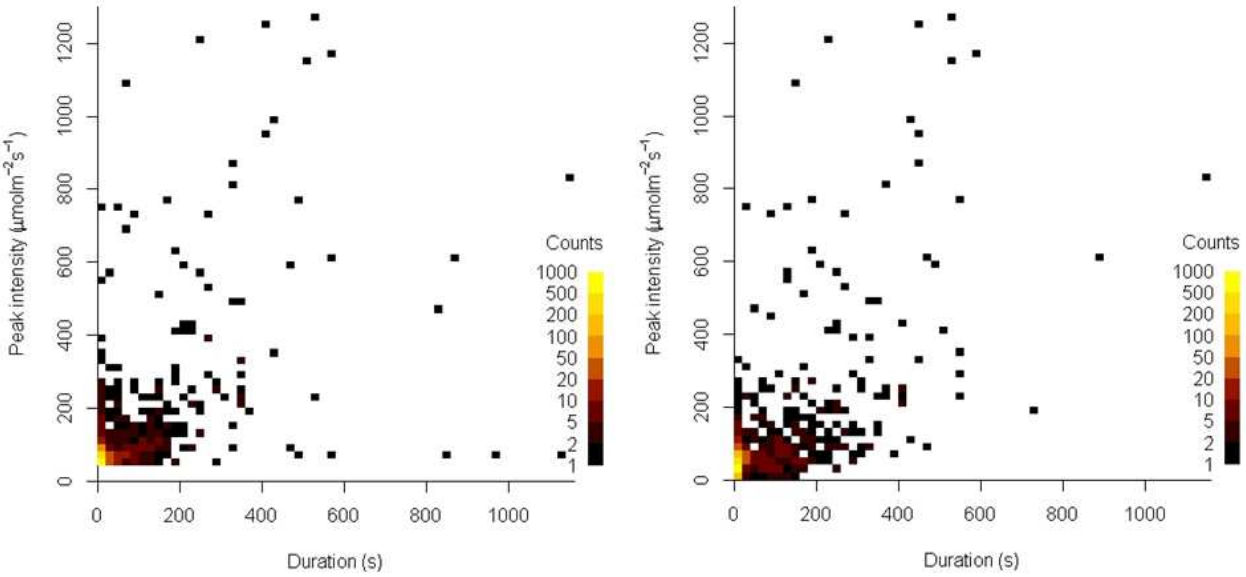

Fig. 2.18 Bivariate histogram of sunfleck duration and peak intensity for sunflecks identified by definition A (left) and definition B (right).

2.4 Discussion and Future Directions

Our results confirm the claim by Ma (2010) that HIA overestimates transmittance relative to direct measurement using BF3 sensors. No correlation was found between daily integrative BF3 estimates and unadjusted HIA estimates of diffuse, direct and total transmittance. This agrees with the finding of Machado and Reich (1999) that HIA is unable to distinguish light availability between microsites in a deeply shaded understory. Weight-adjusted single-day HIA estimates of total transmittance using daily beam fractions calculated with a BF3 sensor performed better than unadjusted HIA estimates, although there was still not a strong correlation with daily integrative BF3 estimates. The adjustment requires an above-canopy sensor that can distinguish between direct and diffuse light, but an approximation could potentially be achieved by modeling the relationship between classes of sky conditions and measured beam fraction.

Tobin and Reich (2009) found that relationships of transmittance indices with average daily estimates differed between forest types. Since our measurements were taken within a relatively small area in one forest stand it is not clear whether our findings can be generalized to other understory environments or forest types. Taken together with other studies, however, it does suggest that HIA should be used with caution under dense canopies. One issue we had in this study was that we found it necessary to hone our image-processing techniques throughout the research process, partly due to lack of previous experience with HIA. This meant that the preliminary distribution of canopy openness values from which we selected our sampling strata might look different if we were to re-analyze the original 5m grid photographs. However, the sampling locations used in this study can still be regarded as randomly chosen from a systematic grid and free from selection bias.

Our comparison of daily integrative BF3 estimates to instantaneous BF3 readings at solar noon questions the reliability of the "less restrictive" method proposed by Paquette et al. (2007). Solar noon estimates were subject to outliers for both diffuse and total transmittance. Diffuse transmittance was generally overestimated on clear days, when there was a higher chance of a sunfleck occurring at solar noon, and underestimated on cloudier days. Total transmittance was generally underestimated except in the case of some strong outliers, likely due to the contribution of direct light events to the daily mean. These issues are similar to those that Sinclair et al. (1974) raised for intermittent sampling. They demonstrated that close to the top of the canopy, deviations of radiation records from the mean were mostly positive, as less frequent sampling tended to overestimate the true mean by failing to record a sufficient number of the relatively few shaded events at that level. Near the bottom of the canopy deviations were mostly negative, as less frequent sampling there tended to underestimate the true mean by failing to include enough of the small number of exposures to direct beam radiation (Péch, 1986).

Although a single instantaneous estimate of transmittance was found to be unreliable, we had better results with 10-minute means selected within two hours of solar noon. Using such averages reduced the effect of outliers, although there was still a fair amount of variation in these 10-minute means around the overall daily mean. The median of several 10-minute means proved to have a strong relationship with the daily integrative BF3 estimate, especially for diffuse transmittance. For researchers with access to BF3 sensors, we recommend estimating daily understory light availability with one sensor above the canopy and at least one sensor below the canopy. The below-canopy sensor(s) can take 10-minute means at a number of locations within two hours of solar noon, and it would be advisable to take several of these 10-minute means at

each location with some time in between them in order to sample a larger range of light values. The median might then be a reasonable estimate of mean daily transmittance.

The choice of methods for characterizing understory light environments should take the plant's perspective into account. This leads us to an important question that requires further investigation: which light metrics best predict plant response? According to Kobe and Hogarth (2007), metrics that integrate direct light may be relatively poor predictors of plant growth, because sunflecks may be above light levels at which photosynthesis saturates. They found that metrics truncating sunflecks to saturation levels improved predictions of white ash radial growth. However, parameters of photosynthesis curves are not static and depend on environmental factors, so adjusting to these parameters might be a challenge. Metrics based on diffuse light may be better predictors of plant response (Tang et al., 1992). There is evidence that diffuse light enhances photosynthesis, that vegetation productivity is sensitive to fluctuations in diffuse light, and that some species may photosynthesize better in diffuse or penumbral light than in direct light (Brodersen et al., 2008; Butt et al., 2010; Smith and Berry, 2013). Researchers are beginning to recognize the importance of diffuse light, and more work is needed in this area. Given the prevalence of cloudy days in the Pacific Northwest and the higher proportion of diffuse light on cloudy days, this is particularly relevant for regions like ours.

Similarly, although we presented a new definition of sunflecks based on diffuse light readings from the BF3 sensor, an improved approach is needed from the plant's perspective. On clear days sunflecks contributed almost half of total available light in our study plot. However, the vast majority of sunflecks were short in duration and low in peak intensity. The physiology of photosynthetic induction and post-illumination photosynthesis is important in situations with shorter exposure durations and lower intensities (Smith and Berry, 2013). Understory plants in such a low-light environment may not have the resources in reserve to utilize such short bursts of direct light efficiently. Response to sunflecks may not be a dominant component of carbon gain in our study area since diffuse light may provide all the energy necessary for photosynthesis. Sunfleck contribution should be based on actual contribution to plant carbon balance, which

must be calculated in relation to induction time, ambient light levels preceding sunflecks and the light saturation point of photosynthesis (Ma et al., in press). In addition, sunflecks are often clustered into periods of multiple sunflecks separated by periods with fewer sunflecks, which could potentially affect carbon gain (Vierling and Wessman, 2000). More investigation is needed into the effects of temporal patterns on sunfleck utilization.

Chapter 3

CHARACTERIZING SPATIAL VARIATION OF UNDERSTORY LIGHT AVAILABILITY USING HEMISPHERICAL IMAGE ANALYSIS AND MOBILE BF3 SENSORS

3.1 Introduction

Understory light heterogeneity is thought to play a major role in carbon gain and survival of regenerating forest seedlings and saplings. There has been much interest in quantifying the spatial variation in understory light environments, with emphasis placed on variations in canopy structure resulting from natural or man-made gaps (Canham et al., 1990; Nicotra et al., 1999). However, Montgomery and Chazdon (2002) suggest that the gap versus non-gap paradigm overlooks the continuum of light levels beneath closed canopy, and that more subtle changes in magnitude and spatial distribution of light beneath closed canopies are also likely to influence long-term survivorship and recruitment of seedlings composing advanced regeneration. Even in relatively uniform stands with a relatively dense canopy there can be significant spatial variation in light transmitted to the understory. Thus, even in stands with few apparent canopy gaps, there are understory positions with higher light regimes that might promote seedling establishment and growth (Lieffers et al., 1998).

Previous efforts to quantify spatial variation of understory light availability have centered around dense spatial sampling using HIA. Collecting HIA estimates of canopy openness or transmittance at a large number of grid points within a study plot enables researchers to create spatial maps of understory light availability. In some cases these are simply contour maps (e.g. Kato and Komiyama, 2002; Motzer, 2005; Poorter and Arets, 2003; Silbernagel and Moeur, 2001; Souza and Martins, 2005), while in other cases spatial interpolation is achieved through kriging (e.g. Battaglia et al., 2002; Hanson and Lorimer, 2007; Raymond et al., 2006; Valladares

and Guzmán, 2005). Besides providing a snapshot of understory light patterns, such maps have been used to compare harvest treatments (Battaglia et al., 2002), to compare different types or layers of forest (Valladares and Guzmán, 2005), to demonstrate seasonal trends (Kato and Komiyama, 2002; Wirth et al., 2001), and to evaluate other models of gap patterns (Silbernagel and Moeur, 2001). Spatial resolution of these maps range from samples at 1m intervals in a study by Valladares and Guzmán (2005) to two random samples per 35 x 35m grid cell in the case discussed by Hanson and Lorimer (2007). Sampling requirements vary between forest stands depending on the spatial scales of variation.

Despite their relative popularity, maps of HIA estimates are problematic for several reasons. Hemispherical photographs cannot be taken at all grid points simultaneously, and although it is unlikely that canopy structure will change substantially during the time required to sample a study plot, minor differences in sky conditions and image exposure could greatly decrease the signal to noise ratio. This is especially important to consider in low-light environments where measurement error can be large relative to the distribution of transmittance values. Furthermore, our results in the previous chapter indicate that under a dense canopy HIA overestimates transmittance relative to direct measurements using BF3 sensors. Thus HIA estimates of understory light availability may be lacking in both precision and accuracy, casting doubt on the value of spatial maps generated from these estimates.

In the present study, in addition to interpolating maps of HIA transmittance estimates, we also investigated the potential of mobile BF3 sensors to quantify spatial variation in understory light. Mobile sampling of understory light is not a new concept. However, the focus has been on averaging over space rather than examining variation in the horizontal plane. Brown (1973)

advocated for spatial integration of transmitted radiation using moving sensors as a more efficient and cost-effective alternative to multiple fixed sensors. Brown demonstrated this approach by moving a pyranometer along a track in a carriage (Fig. 3.1a). Norman and Jarvis (1974) used a radiation sensor driven by a cable-pulley system on two highly tensioned wires to measure average transmittance and transmittance distributions at four heights in Sitka spruce. Following in their footsteps, Sinclair and Knoerr (1982) traversed small sensors at several heights in the canopy of a loblolly plantation. They looked at the distribution of light values at different heights and times of day, and used mean transmittances to produce vertical profiles. Péch (1986) compared mobile and fixed sensors using hourly-integrated records, and concluded that one mobile sensor provided as precise an estimate of below-canopy global radiation as several stationary sensors when averaged for a day. Baldocchi et al. (1984) also used a moving tram system to obtain mean daily values of radiation.

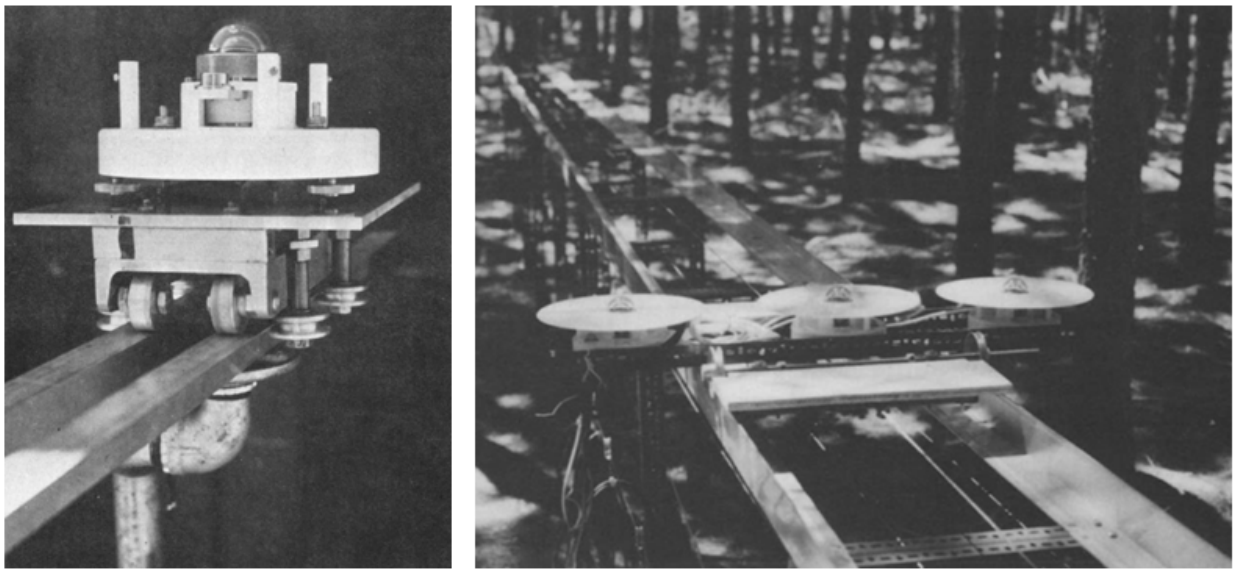

(a) (b)

Fig. 3.1 Mobile sensor systems used in (a) Brown (1973) and (b) Péch (1986).

Mobile systems have been used to examine spatial variation of other environmental variables. Langvall and Orlander (2002) employed the "Asa shuttle" to explore changes in temperature and other meteorological variables along a gradient from clear-cut to un-cut forest. They observed a clear trend along their 400m transect, but this cannot be expected for understory light availability in the absence of such a gradient. Several studies have employed the Networked Infomechanical Systems (NIMS) family of cable-based robotic systems for a variety of applications (e.g. Caron et al., 2008; Graham et al., 2009, 2010; Singh et al., 2007). NIMS is capable of precise positioning within a vertical plane along its span. Singh et al. (2007) used repeated scans of NIMS along a representative transect of a lake to characterize diurnal variation of variables such as temperature, dissolved oxygen and chlorophyll concentration. They also used a robotic boat to perform a surface characterization of the lake.

Inspired by these precedents, we developed the Sequential Quantitative Understory Radiation Logger (SQURL) system to move BF3 sensors along cable line transects within our study plot. The objectives of our study were to (1) characterize the spatial autocorrelation and interpolate maps of understory light availability from HIA estimates of growing season transmittance; (2) characterize the spatial autocorrelation and interpolate maps of seedling density from seedling counts; and (3) explore spatial variation and interpolate maps of understory light availability from repeated scans of the SQURL system. We also raise the question of whether creating maps of understory light availability is a useful endeavor, especially in light of the results in Chapter 2 and the temporal variability we see from the SQURL.

3.2 Methods

3.2.1 HIA grid sampling

Grid points were marked at 5m intervals throughout the entire study plot. In addition, an 18 x 18 m subplot in the northwest corner was marked at 2m intervals, and 19 more points randomly selected within the subplot, for a total of 200 sampling locations overall (Fig. 3.2). The denser spacing in the subplot was employed to improve spatial resolution, and the combination of both regularly spaced and random coordinates was based on sampling designs recommended for geostatistics by Diggle and Ribeiro (2007).

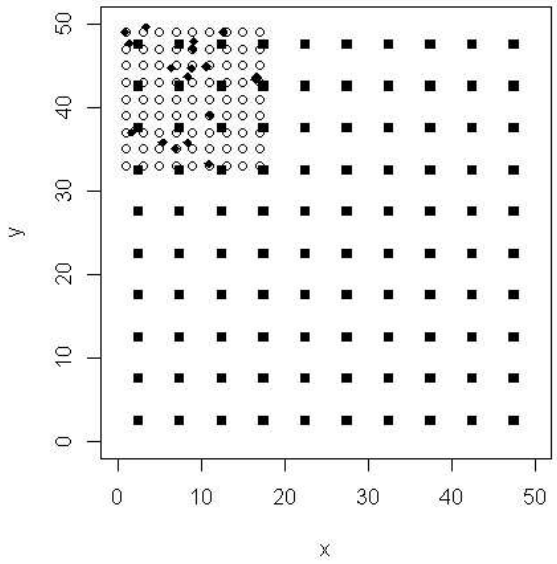

Fig. 3.2 HIA spatial sampling design. 100 points were located on a 5 x 5m grid covering the study plot. Within the northwest subplot, 81 points were located on a 2 x 2m grid with an additional 19 points located randomly.

Hemispherical photographs were taken at each of the sampling locations on a number of overcast days during the Summer 2012 field season, in the same manner as outlined in Section 2.2.2. All photographs were taken at a height of 1.5m above ground and some locations were sampled on more than one day to get an estimate of sampling error. For each set of exposure-bracketed photographs the best possible exposure was chosen to optimize sky-foliage contrast, and much care was taken to ensure consistency of exposures for different spatial locations. This

is a tricky process because an unchanging, uniformly overcast sky is virtually impossible to come across. Even under the most uniform overcast conditions the overall sky brightness was constantly shifting as our photographers moved between locations. To maintain consistency in some cases two exposures were selected for a point and their outputs averaged. Locations with replicates were useful for maintaining a common standard between measurement days.

All of the digital images were automatically thresholded using SideLook 1.1 (Nobis, 2005) and then processed through Gap Light Analyzer 2.0 (Frazer et al., 1999) to obtain estimates of direct, diffuse and total transmittance. Since we were interested in the spatial distribution of understory light availability on average over an extended period of time rather than a single day, the images were analyzed using a growing season from March 1 to November 30. Similarly, the beam fraction was set to the default value of 0.5 since for most regions in North America this is a reasonable approximation on average over the year (Frazer et al., 1999). Region-specific model parameters were set to the values in Table 2.1.

3.2.2 Seedling counts

Seedling counts were recorded in September 2012 at each of the 5m grid points used for HIA sampling. A 1 x 1m square quadrat was placed over each grid point, and seedlings counted by hand inside the quadrat.

3.2.3 The Sequential Quantitative Understory Radiation Logger (SQURL)

In order to achieve a similar level and extent of spatial sampling with our limited number of BF3 sensors, we developed the novel Sequential Quantitative Understory Radiation Logger (SQURL) system. The SQURL system consists of two main components: a motorized tram and a cable setup. The cable setup includes a winch, a pair of cloth tie-down straps, and a sufficient

length of steel cable. The cable can be strung between two trees by wrapping a tie-down strap around each tree and connecting the cable to these straps. The winch is attached between the cable and one of the straps, and used to adjust the tension of the line. The SQURL tram is a battery-powered cart that travels along the tightened cable. The upper portion of the cart sits above the cable and houses a BF3 sensor, while the body of the cart houses the data-logger and the mechanics (Fig. 3.3). A toothed belt runs from the motor to two geared wheels on struts that rest on top of the cable, allowing the tram to move forward along the line at a constant velocity. The SQURL is operated by remote control, which allows the user to adjust the speed and to start or stop motion at any moment. The BF3 sensor may be leveled relative to the ground by adjusting the bolt on the upper housing and/or the fishing weight suspended from the bottom of the cart for improved stability.

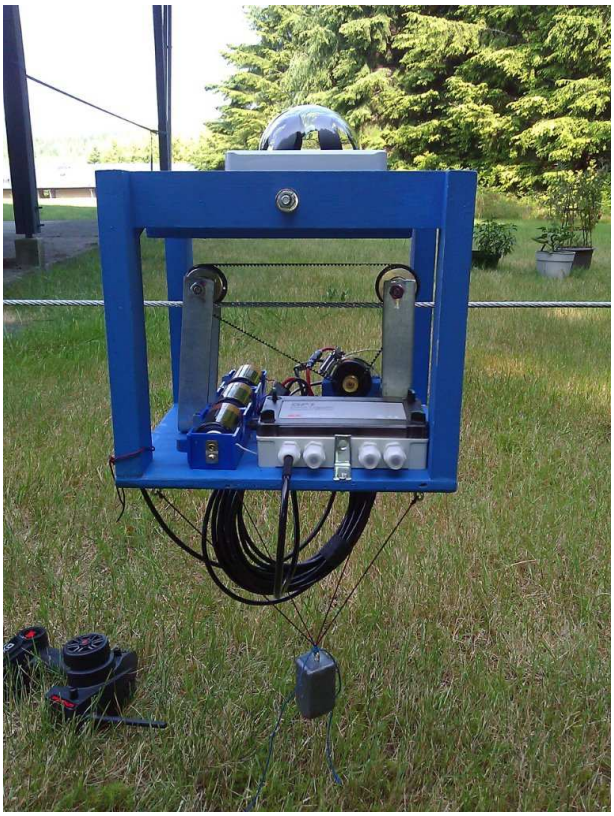

Fig. 3.3 The SQURL system consists of a motorized tram and cable setup. The upper portion of the tram houses the BF3 sensor, while the body contains the data logger and mechanics. The SQURL is operated by remote control.

3.2.4 SQURL line transect sampling

Cable line transects were set up throughout the study plot for sampling with the SQURL, including 12 longer transects in the overall plot and 6 shorter transects to more densely cover the northwest subplot (Fig. 3.4). A portion of one longer transect also fell within the subplot. The placement of the lines depended largely on practical restrictions. For example, the motorized tram had to be able to travel the length of the transect without running into any obstacles. The two endpoint trees also had to be strong enough to sustain the tension from tightening the cable. We tried to make the line transects as long as possible while still able to maintain the high tension necessary for smooth SQURL movement, and to cover as much of the plot area as possible given our cable supply. Lines were selected in a variety of directions in case of anisotropy. The height of each line was approximately 1.5m above ground on average, and starting and ending points were marked with stoppers at fixed distances away from the trees.

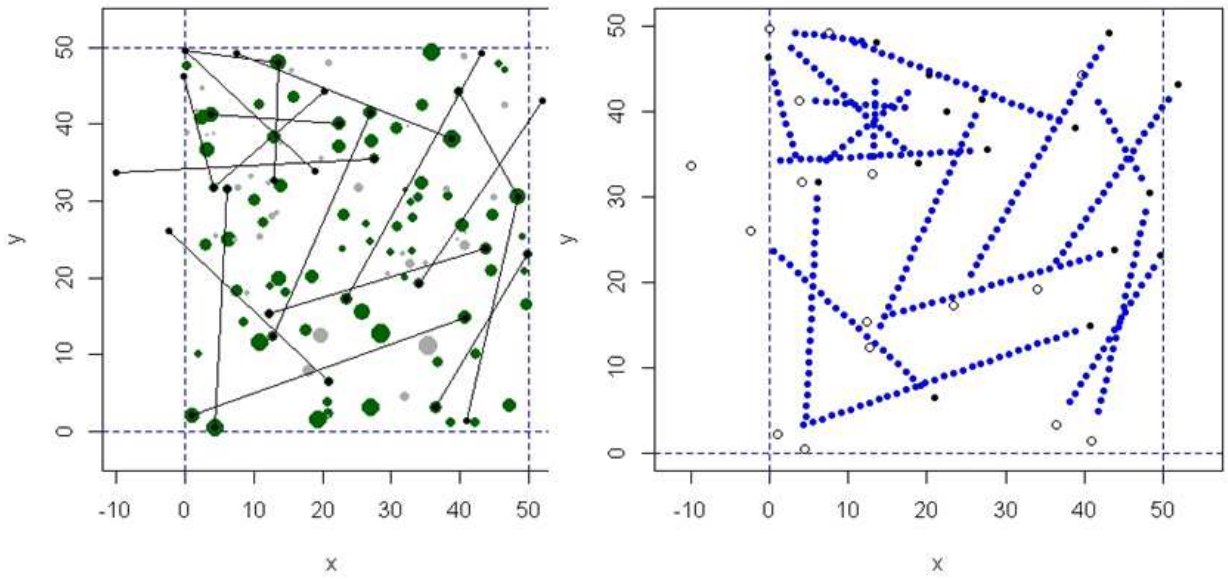

Fig. 3.4 The SQURL sampling design consisted of 18 cable line transects connected between pairs of trees (left). Transmittance estimated from SQURL runs was sampled at regular intervals along each line transect (right).

On each measurement day, one BF3 sensor was stationed and continuously logging light readings at the above-canopy reference site, while another BF3 was mounted on a tripod at a

fixed position within the study plot to log stationary below-canopy light readings. The remaining one or two BF3 sensors were used with the SQURL system to sample as many of the line transects as time allowed. These sensors continuously logged below-canopy light readings while being transported by the motorized tram for a set of multiple runs. All readings were taken at a rate of once per second, and all measurements were made within two hours of solar noon to minimize the effect of changes in solar angle. Each line transect was sampled on several days in August and September of 2012.

The BF3 on the SQURL was covered whenever measurements were not being made. At the start of each SQURL run, the BF3 was leveled at the starting point and the cover removed at the same moment as the tram started running via remote control. The tram was stopped and the cover replaced at the ending point. This procedure was repeated for eight to ten consecutive runs each day, with the tram traveling in the same direction for each run. The majority of the runs were conducted at the slowest constant speed possible (extremely slow speeds caused the tram to jolt) to increase resolution, with a couple runs conducted at a faster speed in case of temporal issues. Any runs experiencing mechanical problems (e.g. running out of battery power) were noted and repeated. Only successful runs were included in the final analysis.

Since BF3 readings were logged continuously each day, change point detection was used to identify the readings associated with SQURL runs. These runs were sampled at regular distance intervals to calculate a predetermined number of transmittance estimates for each line transect, such that these distance intervals corresponded to approximately 1.25m on average (see Fig. 3.4). This enabled comparison of consecutive runs along the same line transect on the same day. Averages were calculated for each line-day, as well as each line over multiple days.

3.3 Results

3.3.1 Spatial variation based on transmittance estimates from HIA

Results are reported for the 5m grid spacing. Growing season diffuse transmittance estimated from HIA at the 5m grid points ranged from 3.7% to 8.5%, direct transmittance ranged from 1.6% to 7.58%, and total transmittance ranged from 3.05% to 7.23% of above-canopy light. Figure 3.5 shows filled contour plots of diffuse, direct and total transmittance. As expected, the spatial distribution of diffuse transmittance was more uniform than that of direct transmittance, but still exhibited areas of lower and higher values. Since beam fraction was set to 0.5, total transmittance was the mean of diffuse and direct transmittance. The frequency distributions of these transmittance estimates did not deviate enough from normality to warrant transformation in the geostatistical analysis (Fig. 3.5).

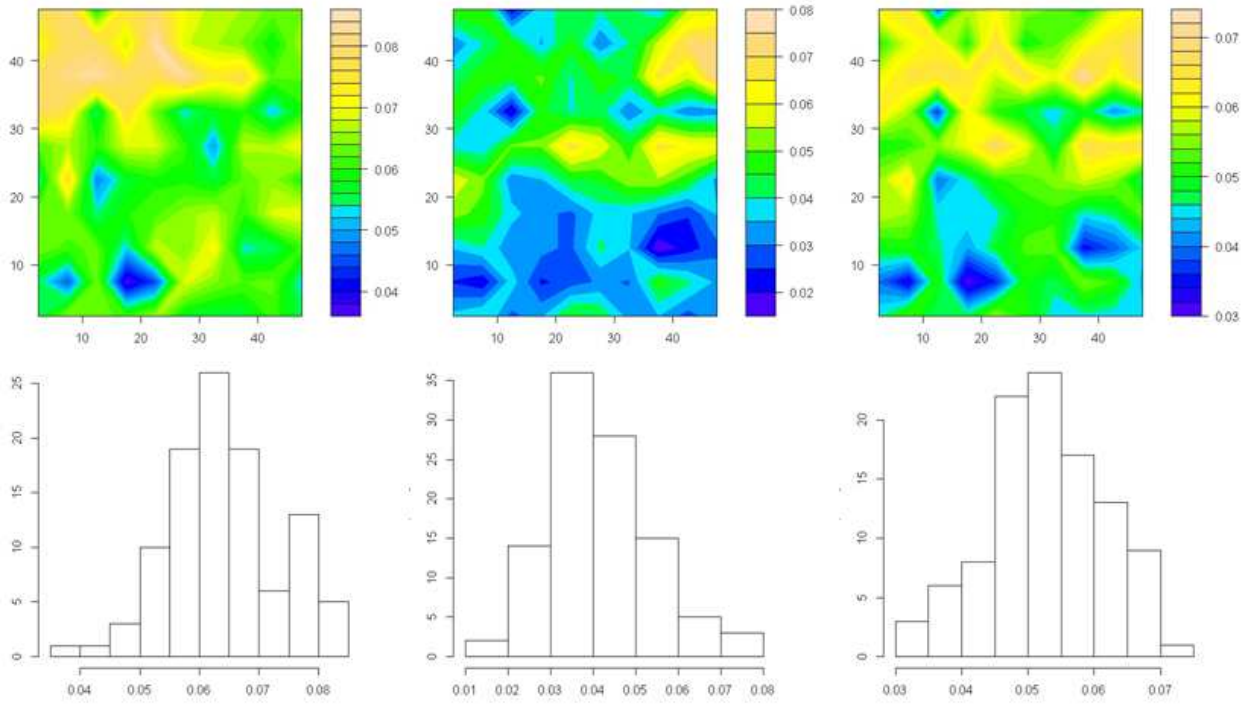

Fig. 3.5 Top: Filled contour plots of diffuse (left), direct (center) and total (right) transmittance estimates from HIA at 5m grid points. Bottom: Corresponding histograms of transmittance estimates do not exhibit strong deviations from normality, so these estimates were not transformed in the geostatistical analysis.

Spatial autocorrelation was modeled by fitting semivariogram functions to empirical semivariograms obtained by plotting half of the squared difference between two observations (the semivariance) against their distance in space, averaged for a series of distance classes with a maximum distance of 30m. There are three basic parameters in semivariograms used to interpret the spatial features of a variable: (1) the *range* is the distance where the semivariance ceases to increase and pairs of observations are considered spatially independent; (2) the *sill* is the semivariance value reached at the range, which is theoretically equivalent to the overall variance of the spatial samples; (3) the *nugget* is the semivariance value at a distance of zero. The empirical semivariograms of the raw transmittance estimates did not quite reach a sill, suggesting the existence of a spatial trend (Fig. 3.6a,b,c). A linear trend surface was fitted, and the empirical semivariograms calculated for the residuals stabilized more strongly around a sill (Fig. 3.6d,e,f).

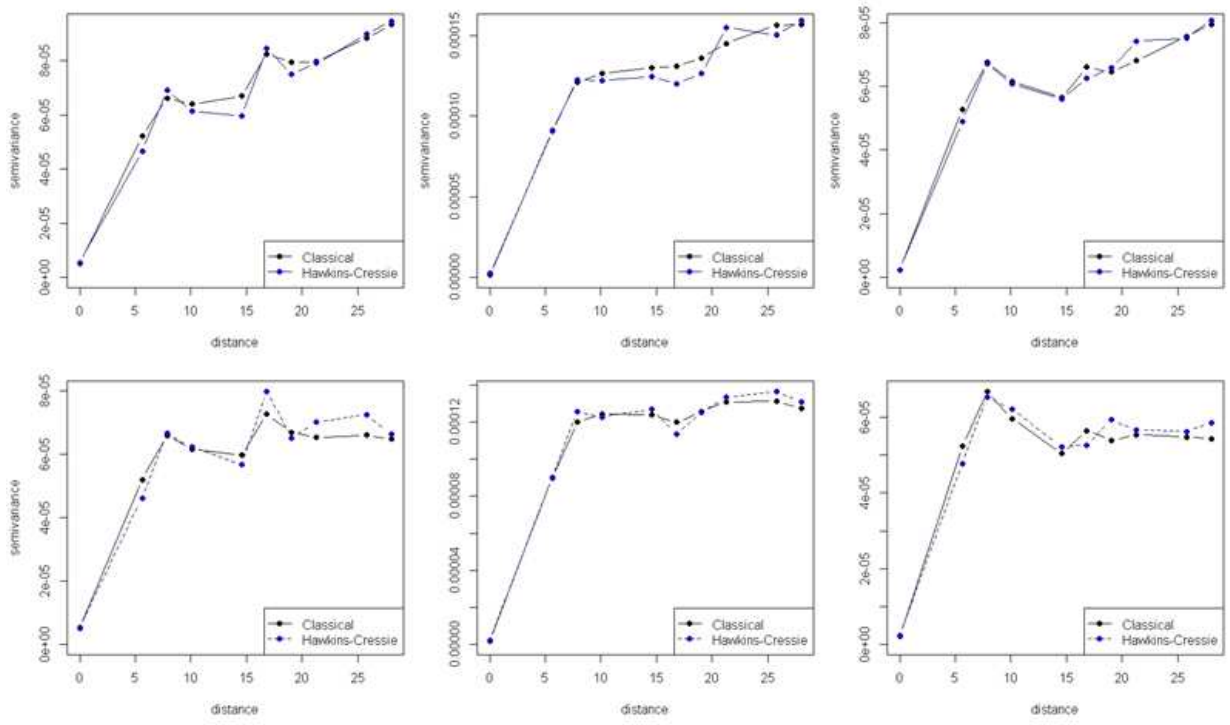

Fig. 3.6 Empirical semivariograms for (top) original transmittance estimates and (bottom) residuals around a fitted linear trend surface (from left: diffuse, direct and total transmittance).

Modeled semivariograms were fitted to the original data as well as residuals around a linear trend surface using the 'likfit' function in geoR (Ribeiro and Diggle, 2001). This function can find maximum likelihood estimates for the parameters of a Gaussian process model:

$$Y(x) = \mu(x) + S(x) + \varepsilon\,, \tag{8}$$

where x defines a spatial location, Y denotes the observed variable, $\mu(x)$ is the mean component of the model, $S(x)$ is a stationary Gaussian process with variance σ^2 (partial sill) and a correlation function parameterized in its simplest form by φ (the range parameter), and ε is the error term with variance parameter τ^2 (nugget variance). Fitted semivariograms including a trend are shown in Figure 3.7 with corresponding parameters in Table 3.1. Exponential models were chosen for diffuse and direct transmittance and a spherical model for total transmittance. The maximum likelihood estimate for nugget variance was zero in all cases because the fitting process did not allow replicate observations. However, since the empirical nugget values were small relative to the average semivariance at a distance of 5m the fits were still quite reasonable, especially for direct transmittance (see Fig. 3.7). For theoretical models with an infinite range the distance at which the semivariogram reaches 95% of the asymptote is called the 'practical range.' The practical range is 3φ for the exponential and φ for the spherical model. Our fitted semivariogram models had practical ranges of 7.4 m, 10.5 m and 6.6 m for diffuse, direct and total transmittance residuals, respectively.

	Covariance model	**β_0**	**β_1**	**β_2**	**τ^2**	**σ^2**	**φ**	**Practical range**
Diffuse	Exponential	0.0591	-0.0001	0.0003	0.0000	0.0001	2.4565	7.3592
Direct	Exponential	0.0305	0.0001	0.0003	0.0000	0.0001	3.5201	10.5453
Total	Spherical	0.0441	0.0000	0.0003	0.0000	0.0001	6.6149	6.6149

Table 3.1 Fitted variogram model parameters using likfit (maximum likelihood estimation) in geoR.

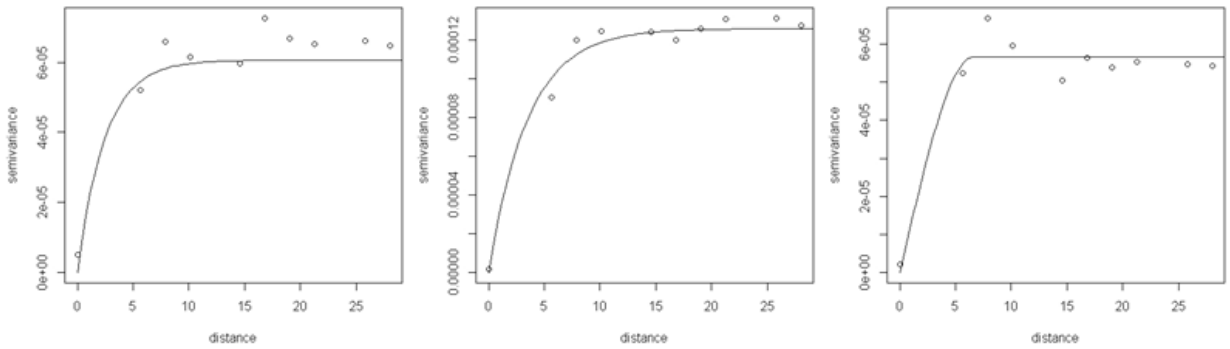

Fig. 3.7 Fitted semivariograms overlaid on empirical semivariograms for diffuse (left), direct (center) and total (right) transmittance residuals around a linear trend surface. Exponential models were used for diffuse and direct transmittance, while a spherical model was fit to total transmittance residuals.

The fitted semivariograms were then used to interpolate maps by kriging (see Fig. 3.8). Spatial heterogeneity of the raw transmittance values had a finer grain for direct than for diffuse transmittance, and total transmittance exhibited a clear gradient with values more similar in the E-W direction than the N-S direction (Fig. 3.8c). Consequently, accounting for a linear trend had a clear effect for diffuse and total transmittance, whereas there was little effect for direct transmittance. Areas of high direct transmittance did not necessarily correspond to areas of high diffuse transmittance, and vice versa, though there did appear to be some consistently low areas.

Another method of interpolation is inverse distance weighting (IDW), where an interpolated point is simply a weighted average of observed values with weights inversely related to distance. This is a deterministic method based on the principle that sample values closer to the prediction location have more influence on the prediction value than sample values farther away. The weights are in the form $\frac{1}{d^k}$, where d is distance and k is a power parameter. Using higher power assigns more weight to closer points resulting in a less smooth, more peaky surface. IDW was used to interpolate maps of HIA transmittance estimates for various values of k (see Fig. 3.9). When k was less than 1, the IDW interpolated maps of diffuse and total transmittance looked similar to their kriged counterparts, with diffuse transmittance exhibiting a decreasing

gradient from the northwest corner to the southern edge of the plot, and total transmittance exhibiting a decreasing gradient from north to south. In contrast to kriging, direct transmittance interpolated by IDW also exhibits a smooth gradient, with higher values in the northeast corner and lower values toward the southern edge. As *k* increased, the interpolated values became more localized and these trends less evident.

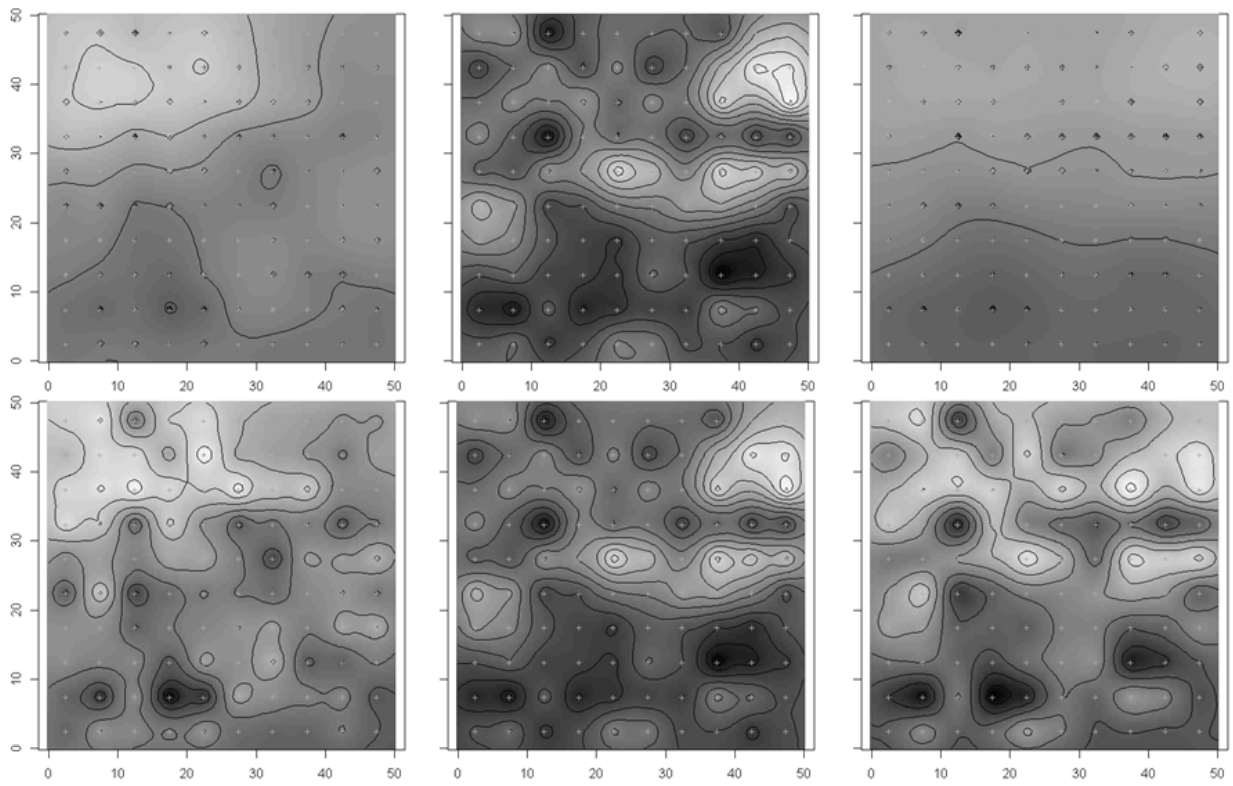

Fig. 3.8 Kriged maps of raw transmittance estimates (top) and residuals around a linear trend surface (bottom). Removing the trend had a clear effect for diffuse (left) and total (right) transmittance, as opposed to direct transmittance (center). Total transmittance exhibited a clear gradient with values more similar in the E-W direction.

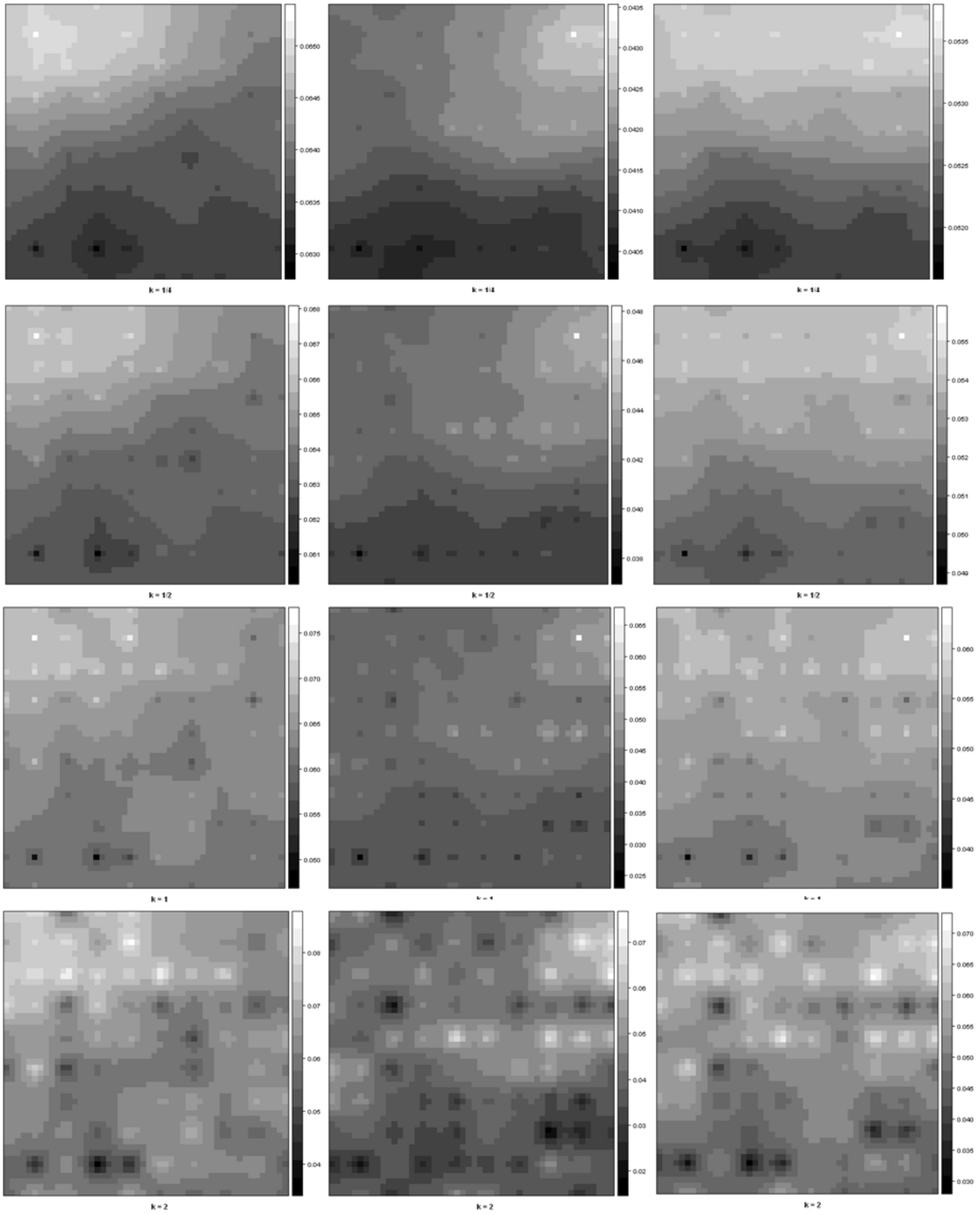

Fig. 3.9 IDW interpolated maps of diffuse (left), direct (center), and total (right) transmittance using smoothing parameter k=0.25 (first row), 0.5 (second row), 1 (third row), and 2 (last row).

We were also interested in seeing if we could have obtained similar results with fewer sampling points. Since direct transmittance had the most resolved semivariogram, we randomly sampled *n* points from the direct transmittance estimates, for *n* = 10, 25 and 50. The only reasonable empirical semivariogram that resulted was for *n* = 50 (see Fig. 3.10). Theoretical semivariogram models were fit to this subsample using maximum likelihood techniques with an exponential covariance function, both with an estimated nugget and with a nugget fixed at zero. When the nugget was estimated the effective range was around 41.7m, whereas when the nugget was fixed at zero the effective range was around 15.3m and the corresponding kriged map more closely resembled that interpolated from all 100 observed points (Fig. 3.11). This illustrates some of the limitations of fitting semivariogram models to experimental data collected at a given scale.

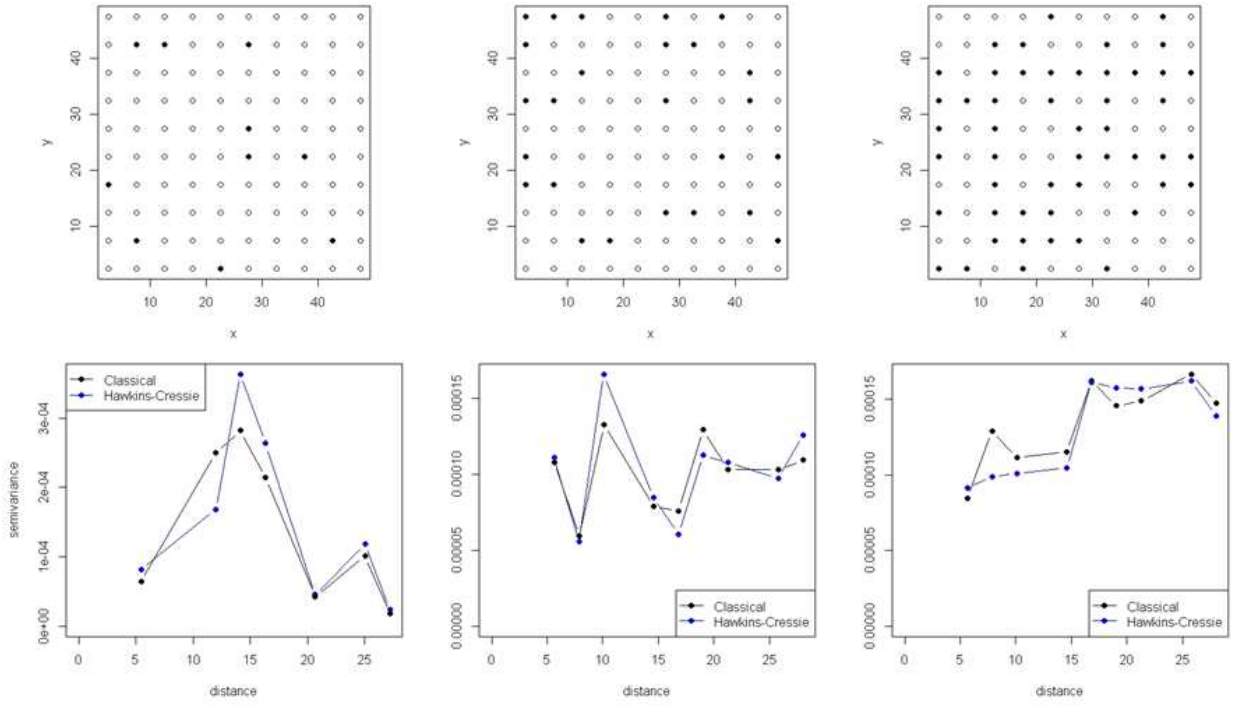

Fig. 3.10 A random subsample from HIA direct transmittance estimates of 10 points (left), 25 points (center) and 50 points (right) with their corresponding empirical semivariograms (bottom).

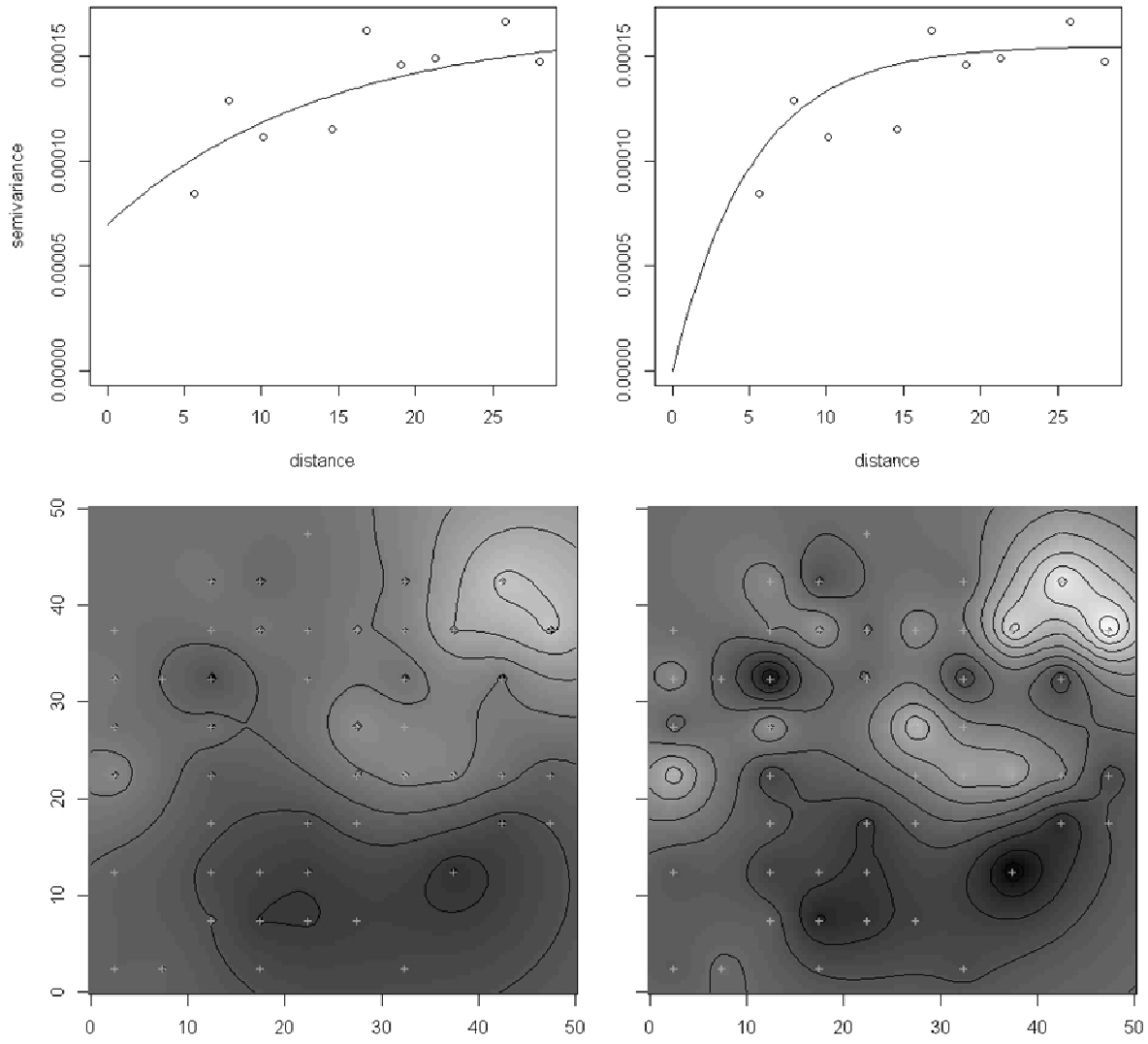

Fig. 3.11 Top: Fitted semivariograms using an exponential model for a random subsample of 50 HIA direct transmittance estimates, with an estimated nugget (left) and with the nugget fixed at zero (right). Bottom: kriged maps using each of these fitted semivariogram models.

3.3.2 Spatial variation of seedling density

Seedling counts in 1 meter square quadrats at the 5m grid points ranged from 1 to 316 seedlings, with a distribution skewed toward lower values (Fig. 3.12c). Spatial heterogeneity had a finer grain for seedling density than for understory light availability. The empirical semivariogram for seedling density shows that spatial correlation was weak to nonexistent, at least at the scale measured (Fig. 3.12a). This is not surprising since qualitative observations indicated that seedling density depended strongly on the presence of organic matter such as decaying logs. The semivariogram fitted with an exponential covariance model using maximum likelihood techniques had a practical range of around 3.4m (Fig. 3.12b). As a result, the map interpolated using ordinary kriging is not very informative (Fig. 3.12d).

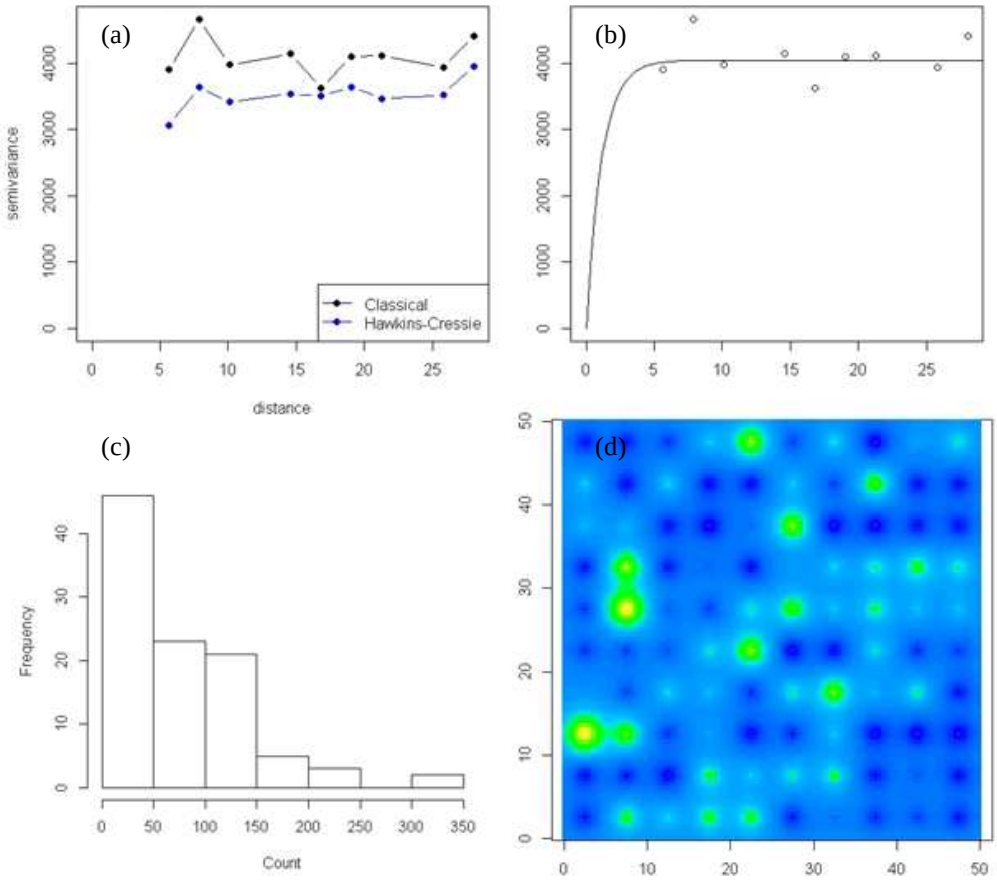

Fig. 3.12 Seedling density was skewed toward lower values (c). Spatial correlation was weak at the scale measured, as seen in empirical (a) and fitted (b) semivariograms and the corresponding kriged map (d).

3.3.3 Spatial variation of diffuse transmittance based on mobile BF3 sensors

There was quite a bit of variation between consecutive runs on the same day, and even more variation between different days, even for diffuse transmittance (e.g. Figs. 3.13, 3.14, 3.15). The results we report here are only for diffuse transmittance, which was less noisy than total transmittance. In some cases the pattern of diffuse transmittance observed along the line transect was quite consistent across measurement days (e.g. Fig. 3.15), whereas in other cases it was not quite as clear (e.g. Fig. 3.13), likely due to differences in weather conditions between the days. A wide range of transmittance values was observed on some of the line transects across days (e.g. Fig. 3.14). In order to obtain a standardized measure for each line transect that could be used for spatial interpolation, each day-average for the transect was centered around zero by subtracting its mean, and then the mean of this relative transmittance was calculated across all measurement days for that line (Fig. 3.16).

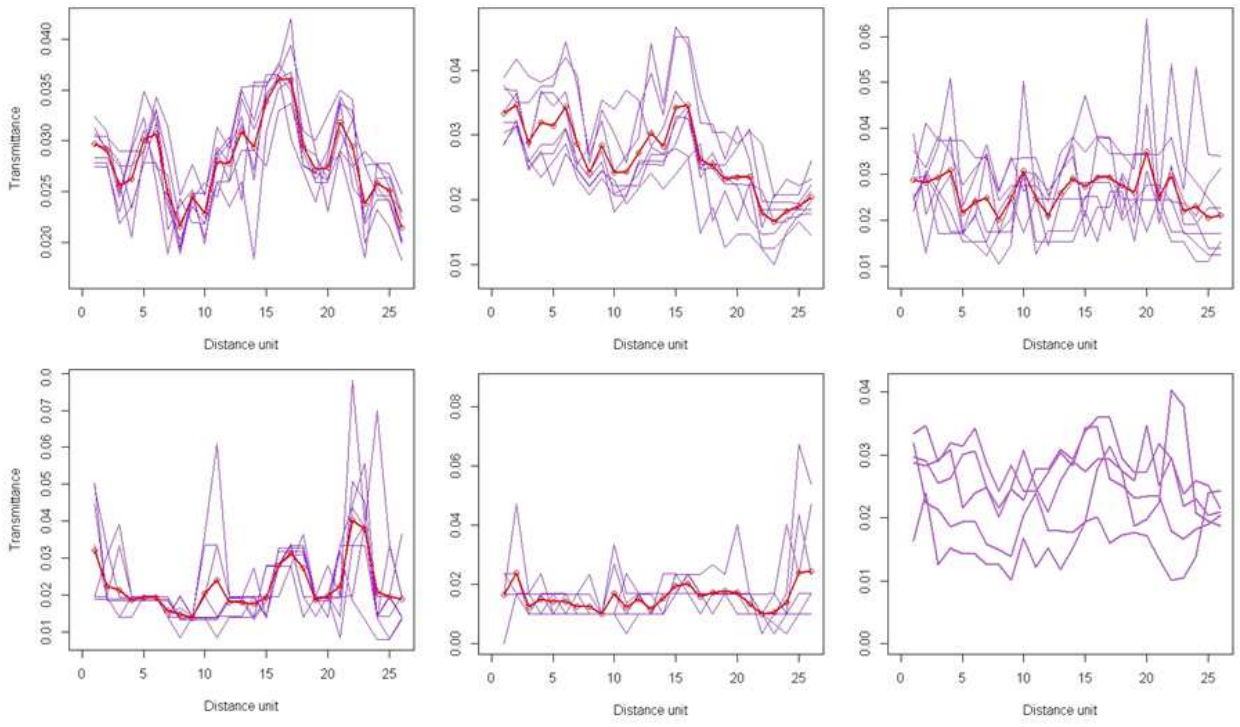

Fig. 3.13 Diffuse transmittance measured along Line F on Aug 27, Aug 30, Aug 31, Sep 5, and Sep 7. Red lines are averages over all runs for each day. The last plot shows all day averages on the same scale.

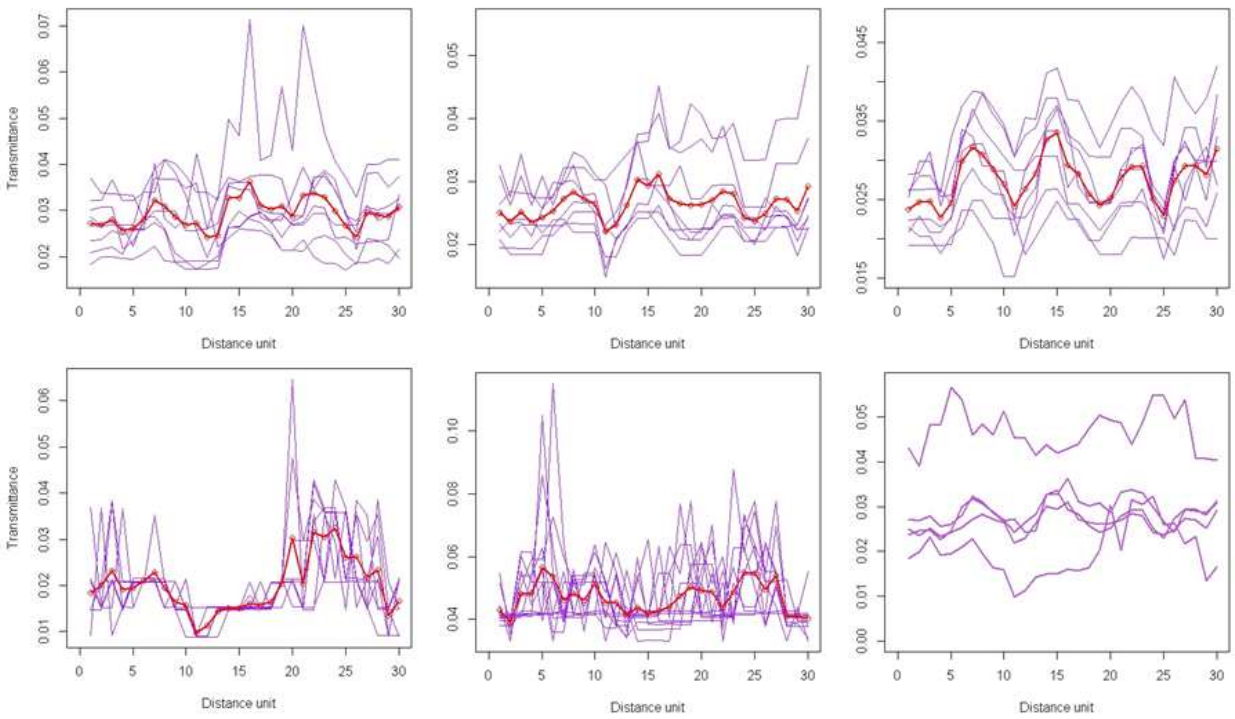

Fig. 3.14 Diffuse transmittance measured along Line D on Aug 22, Aug 23, Aug 30, Sep 5, and Sep 12. Red lines are averages over all runs for each day. The last plot shows all day averages on the same scale.

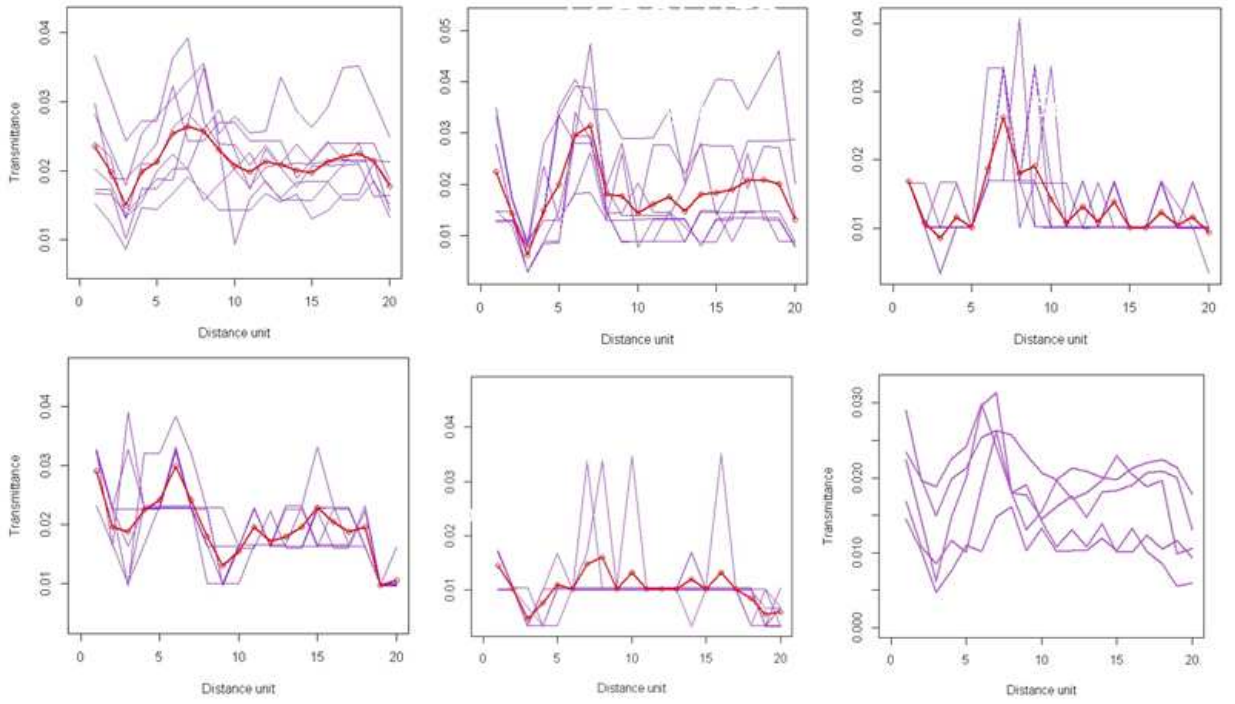

Fig. 3.15 Diffuse transmittance measured along Line C on Aug 23, Aug 31, Sep 4, Sep 5, and Sep 7. Red lines are averages over all runs for each day. The last plot shows all day averages on the same scale.

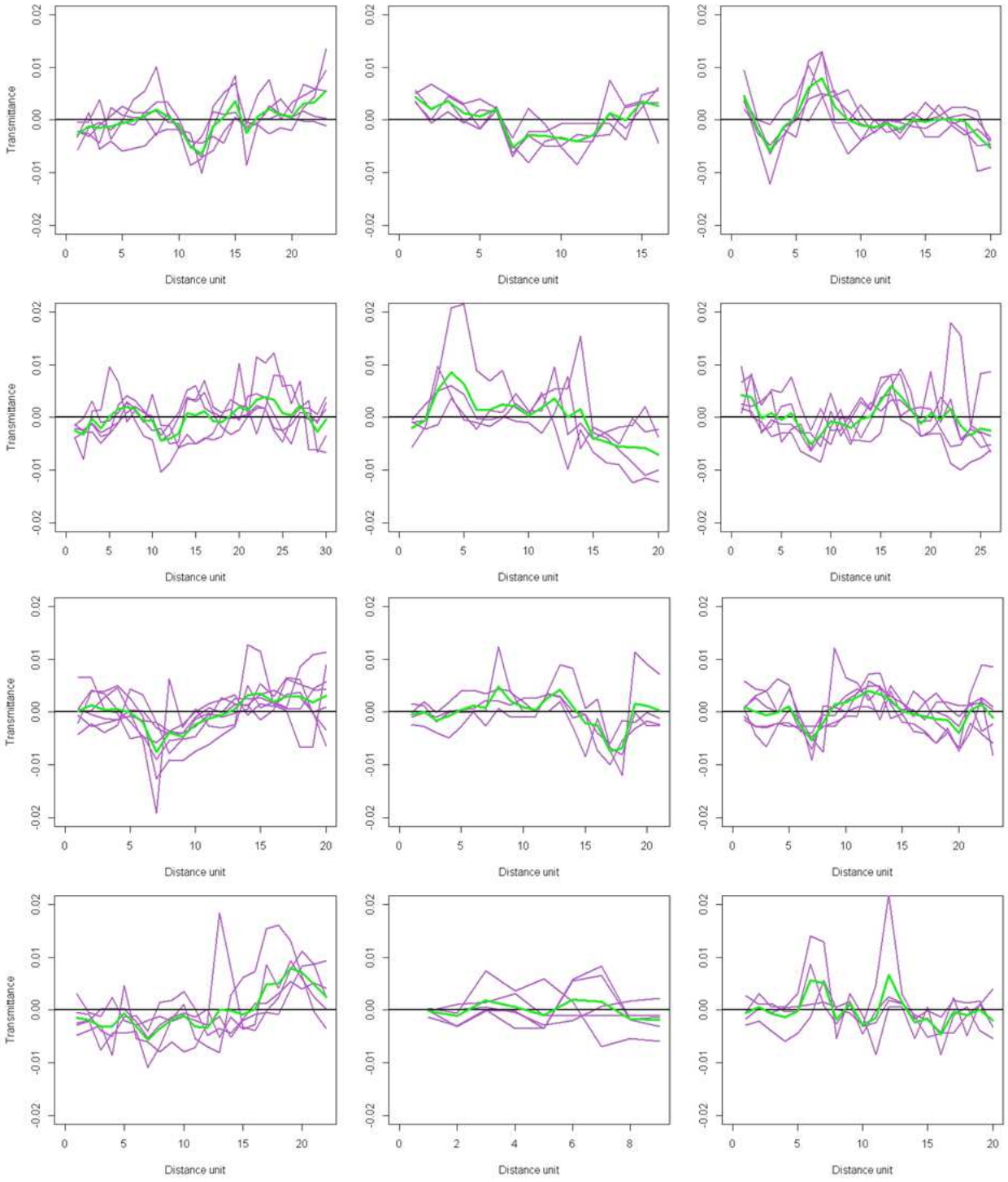

Fig. 3.16 Day-averages (purple) centered around zero for each of the longer SQURL line transects (A-K). The overall average shown in green represents the relative highs and lows along each transect.

Spatial interpolation of these relative diffuse transmittance line-averages was carried out using inverse distance weighting for a range of power parameters (Fig. 3.17). It is important to note that these values are relative separately to the mean transmittance along each line rather than an overall mean for the plot, which allowed the values for each line to be on a similar scale relative to each other. Lighter regions indicate higher transmittance compared to the line means in that area, while darker regions indicate lower transmittance compared to the line means in that area; however it is not clear how regions around different lines relate to each other.

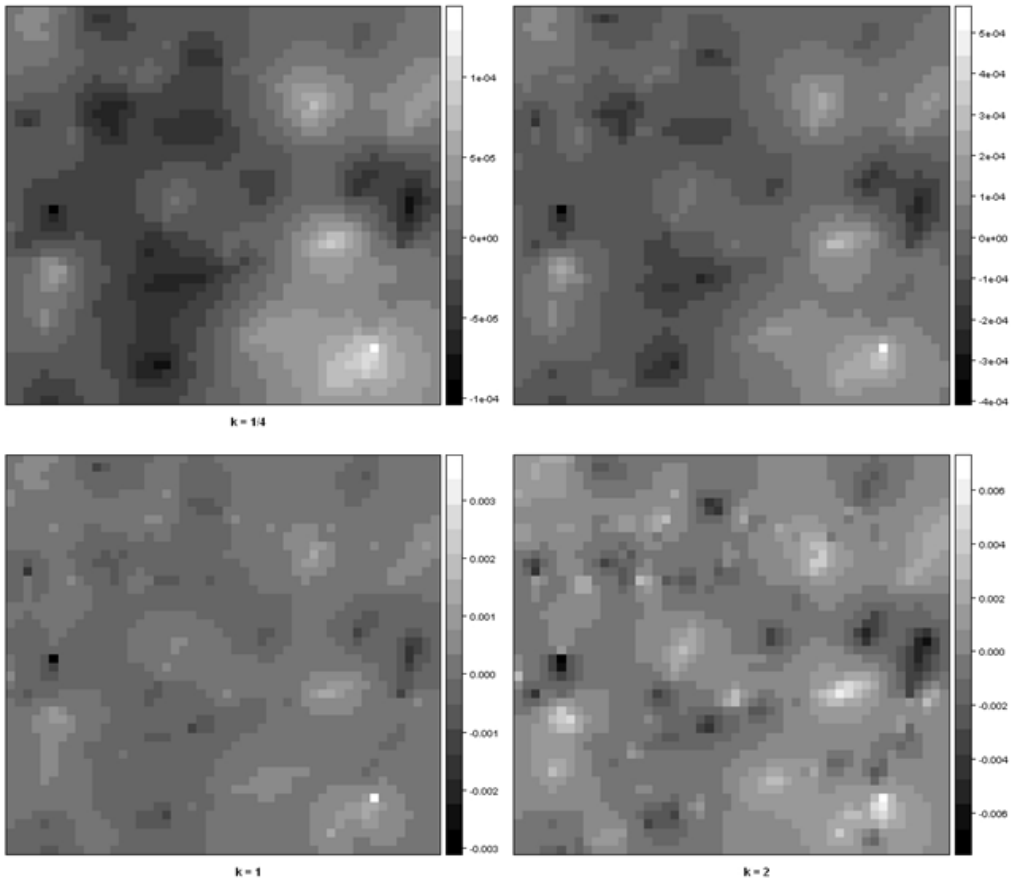

Fig. 3.17 IDW interpolated maps of diffuse transmittance averaged over measurement days and centered around zero, for power parameter k = 0.25, 0.5, 1, 2.

3.4 Discussion and Future Directions

We presented spatial maps of understory light interpolated from HIA estimates of diffuse, direct and total transmittance at 5m grid points. Based on these maps and the accompanying geostatistical analysis, spatial heterogeneity had a finer grain for direct than for diffuse transmittance, and accounting for a linear trend had a greater effect for diffuse transmittance. The fitted semivariogram model for direct transmittance had a reasonable fit and its practical range was around 10.5m. This estimated range is large relative to individual crown sizes, but might reflect overlapping crown structure. Some studies have suggested that range corresponds to mean patch size (Battaglia et al., 2002), while others have questioned such a functional connection. Even if a conceptual connection exists, technical issues limit the interpretability of geostatistical results. Semivariogram analysis may not be able to detect multiple scales of pattern (Meisel and Turner, 1998). In addition, sampling and analysis procedures including choices of lag distance, number of sample pairs for each lag and the semivariogram model chosen can greatly affect estimation of semivariogram range (Guo et al., 2002). Incorporating transmittance estimates made at finer spatial scales within the subplot could shed light on these issues, as could conducting additional analyses on the sensitivity of semivariogram parameters to methods used.

We also analyzed seedling counts made at the same 5m grid points. Seedling density exhibited little spatial autocorrelation at this scale, which is not surprising given observed qualitative patterns. We also measured seedling height for the same seedlings, which may have a stronger relationship with light availability. We plan to investigate this further in future analyses. It might be valuable to conduct a bivariate geostatistical analysis of transmittance and seedling height to explore their relationship in a spatial context. Another interesting future direction

would be to see if there is any relationship between transmittance and some measure of distance to nearest tree weighted by tree size, such as influence potential.

There are several issues with the maps interpolated from HIA transmittance estimates. Our findings in Chapter 2 indicate that HIA has trouble distinguishing between microsites in a low-light environment such as our study plot, and that HIA overestimates transmittance relative to direct measurements by the BF3. Thus the HIA estimates we obtained at the grid points are unlikely to be representative of true understory light availability. The observed spatial structure could be representative of true patterns in canopy structure or light availability, or it could simply be an artifact of our methods. Enough care was taken in the image production and selection process that spatial autocorrelation should be expected. Photographs taken at adjacent grid points tended to be similar not only because of similar canopy structure but also because of similar exposure conditions at moments close together in time and the ease of selecting the same exposure. The observed gradients might be attributable to the fact that we generally took photographs while moving along rows from west to east. We observed small nugget values in empirical semivariograms, but these were based on a small number of replicates, and it would be useful to repeat the analysis with more replicates at the same locations. It would also be interesting to have several different users select image exposures and run the software programs.

Reports of understory light variability using mobile sensors are rare in the literature. The results from our mobile sensor system, the SQURL, show considerable variation in diffuse transmittance values, both between consecutive runs along each line transect as well as between measurement days. This temporal variation of spatial pattern was observed despite the fact that transmittance was calculated relative to above-canopy light values and thus should be accounting

for overall temporal trends. The pattern of transmittance values calculated from the nearby fixed sensor during SQURL runs was generally quite flat, but requires further investigation. It would also be interesting to relate the average transmittance patterns observed to the patterns of trees (or influence potential) along each line transect.

The results from the SQURL system reinforce the complexity and variability of understory light environments. This raises questions about the utility of creating static, smoothed maps of these environments. Future studies employing such maps should take into account the variance highlighted by the SQURL system, and metrics of understory light availability ought to consider interaction between spatial and temporal variation. Moving from physical measurement to biological interpretation, we need to understand how observed patterns in understory light availability affect carbon gain and photosynthesis. How do plants respond to understory light heterogeneity as opposed to mean light availability? We need to build upon existing literature and the present study for an integrated, plant-centric approach to understory light availability, temporal dynamics and spatial variation.

BIBLIOGRAPHY

Baldocchi, D., Collineau, S., 1994. The physical nature of solar radiation in heterogeneous canopies: spatial and temporal attributes, in: Caldwell, M.M., Pearcy, R.W. (Eds.), Exploitation of Environmental Heterogeneity by Plants: Ecophysiological Processes Above- and Belowground. Academic Press, San Diego, pp. 21-70.

Baldocchi, D.D., Matt, D.R, Hutchison, B.A, McMillen, R.T., 1984. Solar radiation within an oak-hickory forest: an evaluation of the extinction coefficients for several radiation components during fully-leafed and leafless periods. Agric. For. Meteorol. 32, 307–322.

Battaglia, M.A., Mou, P., Palik, B., Mitchell, R.J., 2002. The effect of spatially variable overstory on the understory light environment of an open-canopied longleaf pine forest. Can. J. For. Res. 32, 1984–1991.

Brantley, S.T., Young, D.R., 2009. Contribution of sunflecks is minimal in expanding shrub thickets compared to temperate forest. Ecology 90, 1021–9.

Brodersen, C.R., Vogelmann, T.C., 2007. Do epidermal lens cells facilitate the absorptance of diffuse light? Am. J. Bot. 94, 1061–1066.

Brown, G., 1973. Measuring transmitted global radiation with fixed and moving sensors. Agric. Meteorol. 11, 115–121.

Butt, N., New, M., Malhi, Y., da Costa, A.C.L., Oliveira, P., Silva-Espejo, J.E., 2010. Diffuse radiation and cloud fraction relationships in two contrasting Amazonian rainforest sites. Agric. For. Meteorol. 150, 361–368.

Canham, C., 1988. An index for understory light levels in and around canopy gaps. Ecology 69, 1634–1638.

Canham, C., Denslow, J., Platt, W., Runkle, J., Spies, T., White, P., 1990. Light regimes beneath closed canopies and tree-fall gaps in temperate and tropical forests. Can. J. For. Res. 20, 621–631.

Capers, R.S., Chazdon, R.L., 2004. Rapid assessment of understory light availability in a wet tropical forest. Agric. For. Meteorol. 123, 177–185.

Caron, D.A., Stauffer, B., Moorthi, S., Singh, A., Batalin, M., Graham, E.A., Hansen, M., Kaiser, W.J., Das, J., Pereira, A., Dhariwal, A., Zhang, B., Oberg, C., Sukhatme, G.S., 2008. Macro-to fine-scale spatial and temporal distributions and dynamics of phytoplankton and their environmental driving forces in a small montane lake in southern California, USA. Limnol. Oceanogr. 53, 2333–2349.

Cescatti, A., 2007. Indirect estimates of canopy gap fraction based on the linear conversion of hemispherical photographs. Agric. For. Meteorol. 143, 1–12.

Chason, J.W., Baldocchi, D.D., Huston, M.A., 1991. A comparison of direct and indirect methods for estimating forest canopy leaf area Agric. For. Meteorol. 57, 107–128.

Chazdon, R.L., 1998. Sunflecks and their importance to forest understorey plants. Adv. Ecol. Res. 18, 1-63.

Chazdon, R.L., Pearcy, R.W., 1991. The importance of sunflecks for forest understory plants. Bioscience 41, 760–766.

Chen, H.Y., Klinka, K., 1997. Light availability and photosynthesis of Pseudotsuga menziesii seedlings grown in the open and in the forest understory. Tree Physiol. 17, 23–9.

Clearwater, M.J., Nifinluri, T., van Gardingen, P.R, 1999. Forest fire smoke and a test of hemispherical photography for predicting understorey light in Bornean tropical rain forest. Agric. For. Meteorol. 97, 129–139.

Cogliastro, A., Paquette, A., 2012. Thinning effect on light regime and growth of underplanted red oak and black cherry in post-agricultural forests of south-eastern Canada. New Forest. 43, 941–954.

Comeau P.G., Gendron F., Letchford T., 1998. A comparison of several methods for estimating light under a paper birch mixed wood stand. Can. J. For. Res. 28, 1843–1850.

D'Orangeville, L., Bouchard, A., Cogliastro, A., 2011. Unexpected seedling growth in the understory of post-agricultural forests from Eastern Canada. Ann. For. Sci. 68, 759–769.

DeFerrari, C., Naiman, R., 1994. A multi-scale assessment of the occurrence of exotic plants on the Olympic Peninsula, Washington. J. Veg. Sci. 5, 247–258.

Diggle, P.J., Ribeiro, P.J. Jr., 2007. Model-based Geostatistics. Springer, New York.

Engelbrecht, B., Herz, H., 2001. Evaluation of different methods to estimate understorey light conditions in tropical forests. J. Trop. Ecol. 17, 207–224.

Englund, S.R., O'Brien, J.J., Clark, D.B., 2000. Evaluation of digital and film hemispherical photography and spherical densiometry for measuring forest light environments. Can. J. For. Res. 30, 1999-2005.

Evans, G.C., Coombe, D.E., 1959. Hemispherical and woodland canopy photography and the light climate. J. Ecol. 47, 103–113.

Ferment, A., Picard, N., Gourlet-Fleury, S., Baraloto, C., 2001. A comparison of five indirect methods for characterizing the light environment in a tropical forest. Ann. For. Sci. 58, 877–891.

Franklin, J.F., Dyrness, C.T., 1973. Natural Vegetation of Oregon and Washington. Gen. Tech. Rep. PNW-GTR-008. U.S. Department of Agriculture, Forest Service, Pacific Northwest Research Station, Portland, Oregon.

Frazer, G.W., Canham, C.D., Lertzman, K.P., 1999. Gap Light Analyzer (GLA), Version 2.0: Imaging software to extract canopy structure and gap light transmission indices from true-colour fisheye photographs, users manual and program documentation. Copyright © 1999: Simon Fraser University, Burnaby, British Columbia, and the Institute of Ecosystem Studies, Millbrook, New York.

Frazer, G.W., Fournier, R.A., Trofymow, J.A., Hall, R.J., 2001. A comparison of digital and film fisheye photography for analysis of forest canopy structure and gap light transmission. Agric. For. Meteorol. 109, 249–263.

Gendron, F., Messier, C., Comeau, P.G., 1998. Comparison of various methods for estimating the mean growing season percent photosynthetic photon flux density in forests. Agric. For. Meteorol. 92, 55–70.

Geological Survey, 1968. Mean monthly sunshine for selected stations in the United States prepared by U.S. Geological Survey in 1965. The Survey, Washington, D.C.

Graham, E. A., Yuen, E., Robertson, G., Kaiser, W.J., Hamilton, M., Rundel, P., 2009. Budburst and leaf area expansion measured with a novel mobile camera system and simple color thresholding. Environ. Exp. Bot. 65, 238–244.

Graham, E. A., Lam, Y., Yuen, E.M., 2010. Forest understory soil temperatures and heat flux calculated using a Fourier model and scaled using a digital camera. Agric. For. Meteorol. 150, 640–649.

Grayson, S., Buckley, D., Henning, J., Schweitzer, C., Gottschalk, K., Loftis, D., 2012. Understory light regimes following silvicultural treatments in central hardwood forests in Kentucky, USA. Forest Ecol. Manag. 279, 66–76.

Guo, D., Mou, P., Jones, R.H., Mitchell, R.J., 2002. Temporal changes in spatial patterns of soil moisture following disturbance: an experimental approach. J. Ecol. 90, 338–347.

Hale, S.E., Edwards, C., 2002. Comparison of film and digital hemispherical photography across a wide range of canopy densities. Agric. For. Meteorol. 112, 51–56.

Hanson, J.J., Lorimer, C.G., 2007. Forest structure and light regimes following moderate wind storms: implications for multi-cohort management. Ecol. Appl. 17, 1325–40.

Hardy, J.P., Melloh, R., Koenig, G., Marks, D., Winstral, A., Pomeroy, J.W., Link, T., 2004. Solar radiation transmission through conifer canopies. Agric. For. Meteorol. 126, 257–270.

Jonckheere, I., Nackaerts, K., Muys, B., Coppin, P., 2005. Assessment of automatic gap fraction estimation of forests from digital hemispherical photography. Agric. For. Meteorol. 132, 96–114.

Kato, S., Komiyama, A., 2002. Spatial and seasonal heterogeneity in understory light conditions caused by differential leaf flushing of deciduous overstory trees. Ecol. Res. 17, 687–693.

Kobayashi, H., Baldocchi, D.D., Ryu, Y., Chen, Q., Ma, S., Osuna, J.L., Ustin, S.L., 2012. Modeling energy and carbon fluxes in a heterogeneous oak woodland: A three-dimensional approach. Agric. For. Meteorol. 152, 83–100.

Kobe, R.K., Hogarth, L.J., 2007. Evaluation of irradiance metrics with respect to predicting sapling growth. Can. J. For. Res. 37, 1203–1213.

Langvall, O., Örlander, G., 2001. Effects of pine shelterwoods on microclimate and frost damage to Norway spruce seedlings. Can. J. For. Res. 31, 155–164.

Langvall, O., Ottosson Lofvenius, M., 2002. Effect of shelterwood density on nocturnal near-ground temperature, frost injury risk and budburst date of Norway spruce. Forest Ecol. Manag. 168, 149–161.

Lei, T., Lechowicz, M., 1990. Shade adaptation and shade tolerance in saplings of three Acer species from eastern North America. Oecologia 84, 224–228.

Lei, T., Nilsen, E., Semones, S., 2006. Light environment under Rhododendron maximum thickets and estimated carbon gain of regenerating forest tree seedlings. Plant Ecol. 184, 143–156.

Lieffers, V.J., Messier, C., Stadt, K.J., Gendron, F., Comeau, P.G., 1999. Predicting and managing light in the understory of boreal forests. Can. J. For. Res. 29, 796–811.

Ma, Z., 2010. Understory light and its effects in conifer saplings. Unpublished master's thesis, College of Forest Resources, University of Washington.

Ma, Z., Behling, S., Ford, D, in press. Variation in photosynthesis capacity and induction of *Abies amabilis and Tsuga heterophylla* in shaded conditions.

Minkova, T.V., Logan, C.J., 2007. Comparing spherical denisometry and hemispherical photography for estimating canopy closure. The Wildlife Society Annual Meeting, Pendleton, Oregon, 9-13 April.

Machado, JL; Reich, P.B., 1999. Evaluation of several measures of canopy openness as predictors of photosynthetic photon flux density in deeply shaded conifer-dominated forest understory. Can. J. For. Res. 29, 1438–1444.

Meisel, J., Turner, M., 1998. Scale detection in real and artificial landscapes using semivariance analysis. Landscape Ecol. 347–362.

Messier, C., Parent, S., Bergeron, Y., 1998. Effects of overstory and understory vegetation on the understory light environment in mixed boreal forests. J. Veg. Sci. 9, 511–520.

Messier, C., Puttonen, P., 1995. Spatial and temporal variation in the Bight environment of developing Scots pine stands: the basis for a quick and efficient method of characterizing Bight. Can. J. For. Res. 25, 343–354.

Methy, M., Fabreguettes, J., Salager, J., Jardon, F., 1994. A sensor for measurement of spatial heterogeneity of photosynthetically active radiation. J. Agric. Eng. Res. 58, 69–72.

Mölder, M., Lindroth, A., 1999. Thermal roughness length of a boreal forest. Agric. For. Meteorol. 99, 659–670.

Montgomery, R.A., Chazdon, R.L., 2002. Light gradient partitioning by tropical tree seedlings in the absence of canopy gaps. Oecologia 131, 165–174.

Motzer, T., 2005. Micrometeorological aspects of a tropical mountain forest. Agric. For. Meteorol. 135, 230–240.

Nicotra, A., Chazdon, R., Iriarte, S., 1999. Spatial heterogeneity of light and woody seedling regeneration in tropical wet forests. Ecology 80, 1908–1926.

Nobis, M., 2005. SideLook 1.1 - Imaging software for the analysis of vegetation structure with true-colour photographs. http://www.appleco.ch.

Nobis, M., Hunziker, U., 2005. Automatic thresholding for hemispherical canopy-photographs based on edge detection. Agric. For. Meteorol. 128, 243–250.

Paquette, A., Bouchard, A., Cogliastro, A., 2007. A less restrictive technique for the estimation of understory light under variable weather conditions. Forest Ecol. Manag. 242, 800–804.

Parent, S., Messier, C., 1996. A simple and efficient method to estimate microsite light availability under a forest canopy. Can. J. For. Res. 26, 151–154.

Pech, G., 1986. Mobile sampling of solar radiation under conifers. Agric. For. Meteorol. 37, 15–28.

Poorter, L., Arets, E.J.M.M., 2003. Light environment and tree strategies in a Bolivian tropical moist forest: an evaluation of the light partitioning hypothesis. Plant Ecol. 166, 295–306.

Promis, A., Caldentey, J., Cruz, G., 2012. Evaluating the usefulness of hemispherical photographs as a means to estimate photosynthetic photon flux density during a growing season in the understorey of Nothofagus pumilio. Plant Biosyst. 37–41.

Raymond, P., Munson, A.D., Ruel, J.-C., Coates, D.K., 2006. Spatial patterns of soil microclimate, light, regeneration, and growth within silvicultural gaps of mixed tolerant hardwood white pine stands. Can. J. For. Res. 651, 639–651.

Rich, P.M., Clark, D.B., Clark, D.A., Oberbauer, S.F., 1993. Long-term study of solar radiation regimes in a tropical wet forest using quantum sensors and hemispherical photography. Agric. For. Meteorol. 65, 107–127.

Roxburgh, J.R., Kelly, D., 1995. Uses and limitations of hemispherical photography for estimating forest light environments. New Zeal. J. Ecol. 19(2), 213–217.

Rozenbergar, D., Kolar, U., Cater, M., Diaci, J., 2011. Comparison of four methods for estimating relative solar radiation in managed and old-growth silver fir-beech forest. Dendrobiology 65, 73–82.

Silbernagel, J., Moeur, M., 2001. Modeling canopy openness and understory gap patterns based on image analysis and mapped tree data. Forest Ecol. Manag. 149, 217–233.

Sinclair, T.R., Desjardins, R.L., Lemon, E.R., 1974. Analysis of sampling errors with traversing radiation sensors in corn canopies. Agron. J. 66, 214–217.

Sinclair, T.R., Knoerr, K.R., 1982. Distribution of Photosynthetically Active Radiation in the Canopy of a Loblolly Pine Plantation. J. Appl. Ecol. 19, 183.

Singh, A., Stealey, M.J., Chen, V., Kaiser, W.J., Stauffer, B., Moorthi, S., Caron, D., Hansen, M., 2007. Human Assisted Robotic Team Campaigns for Aquatic Monitoring. J. Field Robotics 24, 969–989.

Smith, W.K., Berry, Z.C., 2013. Sunflecks? Tree Physiol. 33, 233–7.

Souza, A.F., Martins, F.R., 2005. Spatial variation and dynamics of flooding, canopy openness, and structure in a Neotropical swamp forest. Plant Ecol. 180, 161–173.

Tabor, R.W., Cady, W.M., 1978. Geologic map of the Olympic Peninsula, Washington. U.S. Geol. Survey Misc. Inv. Map I-994.

Tang, Y., Washitani, I., Iwaki, H., 1992. Effects of microsite light availability on the survival and growth of oak seedlings within a grassland. Bot. Mag. Tokyo 105, 281–288.

Tobin, M.F., Reich, P.B., 2009. Comparing indices of understory light availability between hemlock and hardwood forest patches. Can. J. For. Res. 39, 1949–1957.

Valladares, F., Guzmán, B., 2006. Canopy structure and spatial heterogeneity of understory light in an abandoned Holm oak woodland. Ann. For. Sci. 63, 749–761.

Vierling, L.A, Wessman, C.A., 2000. Photosynthetically active radiation heterogeneity within a monodominant Congolese rain forest canopy. Agric. For. Meteorol. 103, 265–278.

Way, D.A., Pearcy, R.W., 2012. Sunflecks in trees and forests: from photosynthetic physiology to global change biology. Tree Physiol. 32, 1066–81.

Wirth, R., Weber, B., Ryel, R.J., 2001. Spatial and temporal variability of canopy structure in a tropical moist forest. Acta Oecol. 22, 235–244.

Zhang, Y., Chen, J., Miller, J., 2005. Determining digital hemispherical photograph exposure for leaf area index estimation. Agric. For. Meteorol. 133, 166–181.